Target Validation For Neurofibromatosis Type 2 Therapeutics.

2013

Alejandra Guinart
University of Central Florida

TARGET VALIDATION FOR NEUROFIBROMATOSIS TYPE 2 THERAPEUTICS

by

ALEJANDRA M. PETRILLI GUINART
M.S. University of Buenos Aires, 1987
M.S. University of Central Florida, 2010

A dissertation submitted in partial fulfillment of the requirements
for the degree of Doctor of Philosophy
in the Burnett School of Biomedical Sciences
in the College of Medicine
at the University of Central Florida
Orlando, Florida

Fall Term
2013

Major Professor: Cristina Fernández-Valle, Ph.D.

ABSTRACT

Neurofibromatosis type 2 (NF2) is a benign tumor disease of the nervous system. Development of bilateral vestibular schwannomas is characteristic of NF2; however patients frequently present schwannomas on other nerves, as well as meningiomas and ependymomas. Currently, there are no drug therapies for NF2. There is an urgent need for development of NF2 therapeutics and this dissertation presents two independent potential therapeutic targets.

The disease is caused by mutations in the *NF2* gene that encodes a tumor suppressor called merlin. Loss of merlin function is associated with increased activity of Rac and p21-activated kinases (PAK) and deregulation of cytoskeletal organization. LIM domain kinases (LIMK1 and 2) are substrates for Cdc42/Rac-PAK, and modulate actin dynamics by phosphorylating cofilin, an actin severing and depolymerizing agent. LIMKs also translocate into the nucleus and regulate cell cycle progression. Here we report that mouse Schwann cells (MSCs) in which merlin function is lost as a result of *Nf2* exon2 deletion ($Nf2^{\Delta Ex2}$) exhibited increased levels of LIMK1, LIMK2, and active phospho-Thr508/505-LIMK1/2, as well as phospho-Ser3-cofilin, compared to wild-type normal MSCs. Similarly, levels of LIMK1 and 2 total protein and active phosphorylated forms were elevated in human vestibular schwannomas compared to normal human Schwann cells (SCs). Reintroduction of wild-type *NF2* into $Nf2^{\Delta Ex2}$ MSC reduced LIMK1 and LIMK2 levels. Pharmacological inhibition of LIMK with BMS-5, decreased the viability of $Nf2^{\Delta Ex2}$ MSCs in a dose-dependent manner, but did not affect viability of

control MSCs. Similarly, LIMK knockdown decreased viability of *Nf2*$^{\Delta Ex2}$ MSCs. The decreased viability of *Nf2*$^{\Delta Ex2}$ MSCs was due to inhibition of cell cycle progression as evidenced by accumulation of cells in G_2/M phase. Inhibition of LIMKs arrest cells in early mitosis by decreasing Aurora A activation and cofilin phosphorylation.

To increase the search for NF2 therapeutics, we applied an alternative approach to drug discovery with an unbiased pilot high-throughput screen of the Library of Pharmacologically Active Compounds. We assayed for compounds capable of reducing viability of *Nf2*$^{\Delta Ex2}$ MSC as a cellular model for human NF2 schwannomas. AGK2, a SIRT2 (sirtuin 2) inhibitor, was identified as a candidate compound. SIRT2, a mammalian sirtuin, is a NAD^+-dependent protein deacetylase. We show that *Nf2*$^{\Delta Ex2}$ MSC have higher expression levels of SIRT2 and lower levels of overall lysine acetylation than wild-type control MSC. Pharmacological inhibition of SIRT2 decreases *Nf2*$^{\Delta Ex2}$ MSC viability in a dose dependent manner without substantially reducing wild-type MSC viability. Inhibition of SIRT2 activity in *Nf2*$^{\Delta Ex2}$ MSC causes cell death accompanied by release of the necrotic markers lactate dehydrogenase and high mobility group box 1 protein into the medium in the absence of significant apoptosis, autophagy, or cell cycle arrest.

Overall this work uncovered two novel potential therapeutic targets, LIMK and SIRT2 for NF2 and tumors associated with merlin deficiency.

I dedicate this dissertation to my parents, Lina and Osvaldo, my sons Phillip and Luc, my sister Monica and my nephew Danny. Thank you for your unconditional support, I could not have done it alone. Your love, confidence and patience gave me the strength to achieve this dream.

ACKNOWLEDGMENTS

First and most I thank my mentor, Dr. Cristina Fernández-Valle. She showed me integrity and taught me to become a round scientist, her support, encouragement and inspiration are unpaired.

I thank my committee members Dr. Stephen Lambert, Dr. Annette Khaled and Dr. Deborah Altomare for their guidance and support. I thank all my UCF friends and Dr. Fernández-Valle laboratory members who share my journey, specially my guardian angel Marga Bott.

This work was supported in part by a NIH (5R01DC10189), a Children's Tumor Foundation-Drug Discovery Award to Dr. C. Fernández-Valle. Additionally I thank the support of the Children's Tumor Foundation through the Young Investigator Award.

Data from Chapter two was first published in the journal ONCOGENE, by Petrilli, A., Copik, A., Posadas, M., Chang, L. S., Welling, D. B., Giovannini, M. & Fernandez-Valle, C. (2013) "LIM domain kinases as potential therapeutic targets for neurofibromatosis type 2" and can be found at http://www.nature.com/onc/journal/vaop/ncurrent/full/onc2013320a.html

TABLE OF CONTENTS

LIST OF FIGURES

LIST OF ABBREVIATIONS

APC/C……..Anaphase Promoting Complex/Cyclosome

BSA……..Bovine Serum Albumin

Cdc42……...Cell Division Cycle protein 42

CREB……cAMP Response Element-Binding protein

DMSO……..Dimethyl Sulfoxide

DNA……..Deoxiribonucleic Acid

FDA……..Food and Drug Administration

GAPDH……Glyceraldehyde-3-Phosphate Dehydrogenase

HDAC6……Histone Deacetylase 6

HIFBS……..……Heat Inactivated Fetal Bovine Serum

HMGB1……High Mobility Group Box 1 protein

HTS……...High Throughput Screen

LC3B-II……..Microtubule-associated protein 1 Light Chain 3 B

LDH……..….Lactate Dehydrogenase

LIMK…….…….LIM domain Kinases

LOPAC……Library of Pharmacologically Active Compounds

MRCK……Myotonic dystrophy kinase-Related Cdc42-binding Kinase

MSC…….…….Mouse Schwann Cells

NF2……Neurfibromatosis Type 2

NF2……Neurfibromatosis Type 2 human gene

NIH…….…..…..National Institute of Health

PAK……..……..p-21-Activated Kinase

PLL……..……..Poly-L-Lysine

PP1……...Protein Phosphatase 1

RIP1……..…….Receptor-interacting protein 1

RIP3……..…….Receptor-interacting protein 3

ROCK……..…..Rho-associated kinases

SDS……..Sodium Dodecyl Sulfate

Sir2……..…..Silent Information Regulator 2

SIRT2……Sirtuin 2

SSH……..…….Slingshot

TNF-α……..……..Tumor Necrosis Factor-alpha

CHAPTER ONE: INTRODUCTION

Neurofibromatosis Type 2

Neurofibromatosis type 2 (NF2) is a genetic disorder that causes multiple tumors to form in the nervous system. Because the incidence rate for NF2 is one in 25,000, it is considered a rare disease. NF2 is inherited in an autosomal dominant manner, however more than half of the patients present with no family history and have *de novo* mutations. The distinctive feature of NF2 is the formation of bilateral vestibular schwannomas, tumors arising from Schwann cells on the vestibular branch of the eighth cranial nerve, the auditory nerve. Patients frequently develop schwannomas in other cranial, spinal and peripheral nerves. Other occurring nervous system tumors are meningiomas and ependymomas [1]. Common initial and progressive symptoms are hearing loss, tinnitus and dizziness. Other symptoms depend on the location of the tumors and include headaches, seizures, pain, paraesthesia, skin plaques and ocular manifestations such as lens opacities and cataracts. The majority of patients will develop axonal neuropathy and present for example facial palsy, foot drop, and muscular weakness that can progress to severe muscle wasting. Although tumors are benign; their growth may compress essential structures such as the brainstem carrying more serious complications including death [1, 2]. The onset of symptoms in NF2 is at a young age, generally between the ages of 18 to 30 years, but children as young as 2 years have manifested with the disease. The diagnosis relies on clinical features, the most widely used is the Manchester diagnostic criteria, which modifies the NIH criteria,

including patients without family history who develop multiple schwannomas and/or meningiomas but have not yet developed bilateral vestibular schwannomas. The NIH original criteria involved patients with bilateral vestibular schwannomas or family history of NF2 plus unilateral vestibular schwannoma or two of any schwannoma, meningioma, glioma, neurofibroma, or lenticular opacities [2, 3]. Currently, microsurgery and stereotactic radiosurgery are the only treatments available to NF2 patients. Surgical removal of the tumors results in deafness and very frequently facial paralysis as well, whereas radiotherapy carries the associated risk of radiation-induced malignant transformation. Additionally some patients are poor surgical candidates; therefore NF2 patients are in need of alternative drug treatment [1, 2].

The work described in this dissertation is focused on validating two targets for development of treatments for NF2. One target, LIMK emerged from knowledge of signaling pathways deregulated in Schwann cells with loss of merlin function. The second target, SIRT2 emerged from an unbiased chemical genomic approach using an *Nf2*$^{\Delta Ex2}$ mouse Schwann cell line in a high throughput screen (HTS) of a compound library.

Merlin

Twenty years ago the *NF2* gene was cloned and mutations in the gene are responsible for NF2 [4, 5]. The tumor suppressor gene *NF2* is located on chromosome 22q12.2 and encodes for a protein called merlin or schwannomin. Merlin is a cytoskeleton associated protein, member of the ERM (ezrin, radixin, moesin) family of

proteins. Merlin regulates cell size, morphology, motility, proliferation, and survival [6, 7]. There are multiple isoforms of human merlin but two alternative isoforms are the most abundant and studied: merlin isoform 1, a 595 amino acids protein that lacks exon 16 from the 17 potential exons and merlin isoform 2, a 590 amino acid protein that includes exon 16 but lacks exon 17. Phosphorylation of merlin at various serine and threonine residues regulates its conformation (growth-permissive or -inhibitory conformation), interaction with binding partners, and sub-cellular localization [7]. Work from Dr. Fernandez-Valle's laboratory has shown that activation of the β1-integrin and ErbB2 receptors with laminin and neuregulin promotes protein kinase A- and p-21-activated kinase (PAK)-dependent phosphorylation of merlin at serine-518, respectively in normal Schwann cells [8]. Years of research from multiple groups have shown merlin's involvement in numerous signaling cascades (Figure 1) including: RasGTPase, the PI3K/AKT/mTOR pathway, mitogenic and cell adhesion receptors (EGFR, ErbB2, CD44, E-cadherin), extracellular matrix receptors (β1 integrins), and the newly-described MST1/2-YAP pathway (Hippo pathway) that controls organ development and homeostasis [5-7, 9, 10]. Merlin also translocates into and accumulates in the nucleus. There merlin inhibits the E3 ubiquitin ligase CLR4 (DCAF1) inducing growth suppression [11].

Merlin negatively regulates Rac1 signaling via inhibition of p21-activated kinases (PAK) [12]. Conversely, activated Rac/cell division cycle protein 42 (Cdc42) binds PAK that phosphorylates and inactivates merlin tumor suppressor activity [12, 13]. Importantly, increased levels of activated Rac and its downstream effector PAK were

reported in primary human schwannoma cells [14]. Studies of PAK inhibitors as potential NF2 therapeutics have shown them capable of reducing schwannoma cell proliferation; however, the vast numbers of PAK substrates reduces its likelihood in clinical applications. Thus selectively targeting a key downstream PAK effector would be more desirable [15]. Among PAK substrates are the LIM domain kinases, terminal kinases in the Rac/Cdc42/PAK/LIMK/cofilin pathway and as such potential targets for NF2 therapy.

LIM Domain Kinases

The LIM domain kinases (LIMK) are serine/threonine protein kinases that contain two LIM domains at their N-terminus, which each contain two zinc fingers, followed by a PDZ domain and the kinase domain at the C-terminus. The LIMK family has two members, LIMK1 and LIMK2 that are highly related and encoded by separate genes. Human *LIMK1* gene is located on chromosome 7q11.23, and human *LIMK2* gene is on chromosome 22q12.2 [16].

LIM kinases, like other kinases, when phosphorylated in the activation loop increase their enzymatic activity despite the presence of other regulatory phosphorylation sites. LIMK1 is activated by Thr-508 phosphorylation and LIMK2 by Thr-505 phosphorylation. Both LIMK can be phosphorylated by Cdc42/Rac effectors-PAK1, 2 and 4 to become active serine/threonine kinases (Figure 1). LIMK are also activated by other small GTPase downstream effectors including the Rho effectors Rho-associated kinases 1 and 2(ROCK1 and 2) and the Cdc42 effector myotonic dystrophy

kinase-related Cdc42-binding kinase (MRCK) [16, 17]. Conversely, LIMK are inactivated by the phosphatase slingshot (SSH) that also dephosphorylates cofilin and by ubiquitin-induced proteosomal degradation by the E3 ubiquitin ligases Rnf6 and parkin [18-20].

The most study and characterized LIMK substrate is the actin depolymerizing and severing protein, cofilin. Here, the general term cofilin refers to cofilin1(alternatively called non-muscle cofilin), as opposed to cofilin2 (muscle cofilin) and destrin (commonly known as actin depolymerization factor ADF). LIMK phosphorylation of cofilin at Ser-3 inactivates its actin depolymerizing and severing function. Thus, cofilin Ser-3 phosphorylation promotes stabilization of the actin cytoskeleton [21]. Although cofilin is the major LIMK substrate, more recently other substrates have been identified. The cAMP response element-binding protein (CREB) transcriptional factor is phosphorylated at Ser-133 by LIMK1 upon fibroblast growth factor-2 stimulation via the Rac/Cdc42/PAK1 pathway in hippocampal neuron progenitor cells during differentiation [22]. Additionally, among the multiple signaling pathways that regulate the transcriptional activity of the orphan nuclear receptor Nurr1, LIMK1 directly interacts with Nurr1 and negatively regulates its activity [23]. Lastly, LIMK1 phosphorylates and is a substrate for Aurora A to promote its activation and autophosphorylation at Thr-288 [24] whereas LIMK2 is an Aurora A substrate and stabilizes it depending on both its kinase and scaffolding actions [25].

Reorganization of the actin cytoskeleton by LIMK actions on cofilin in the cytoplasm and in focal adhesions modulates cell morphology and motility. LIMK's role in morphology was extensively studied in neurons and its importance is revealed by the

abnormal morphology of spines and greatly reduced growth cones in hippocampal neurons of the *Limk1* knockout mice, consequently presenting abnormalities in the synaptic function [26]. Moreover, in the *Limk1*- *Limk2* double knockout mice, long term potentiation and synaptic response were more severely altered [27].

LIM domain kinases also have a role in cell cycle and cytokinesis. Through progression of the cell cycle LIM kinases show distinctive subcellular localization, they translocate to the nucleus and centrosome regulating mitotic spindle organization, centrosome division and chromosome segregation, and to the cleavage furrow influencing cytokinesis [16]. During mitosis LIMK activity varies from prophase to metaphase the level of LIMK1 activity increases to favor phosphorylation of cofilin; while during anaphase and telophase LIMK1 activity gradually returns to basal levels [28-30]. Interestingly, both LIM kinases functionally interact with aurora A kinase that regulates centrosome dynamics, spindle assembly and chromosome alignment and segregation [31, 32]; In early mitosis phospho-LIM kinases co-localize with γ-tubulin in the centrosomes, in metaphase LIMK1 is found at the spindle poles and later redistributes to the cleavage furrow. In contrast, LIMK2 localizes along the spindle and at the cleavage furrow of post-mitotic cells [24, 25].

Both LIM kinases are widely expressed in tissues of embryonic and adult mice showing a temporal dynamics and with similar distribution except for the testis where their expression is complementary. LIMK1 was expressed at higher levels in the spermatocytes, Sertoli cells and early spermatids than in mature spermatids. LIMK2 was found only in the mature elongated spermatids [33-35]. Microdeletion of several

genes on chromosome 7q11.23 including *LIMK1* is associated with a mental disorder called Williams syndrome. Williams syndrome patients present severe visuospatial cognition impairment, moderate mental retardation or learning disabilities. Importantly, LIMK are implicated in other diseases, including cancer. Several reports show LIMK overexpression in various cancers, including breast, lung, skin, liver and prostate, as well as various tumor cell lines [36-39]. Therefore, LIMKs are emerging potential targets for cancer therapy [40].

SIRT2

SIRT2 or sirtuin2 is one of the seven identified mammalian sirtuins. Sirtuins are deacetylases that remove the acetyl group from the epsilon-amine of lysines from proteins and belong to the class III histone deacetylases (HDACs). HDAC proteins are now also called lysine deacetylases (KDAC) to more appropriately describe their function instead of their target, because they also deacetylate non-histone proteins [41]. Based on their homology to yeast proteins, mammalian HDACs are classified into three groups. Class I and II include HDACs with homology to the yeast RPD3 and HDA1 respectively. The class III includes the sirtuins that are homologous to the yeast Sir2 (silent information regulator 2) [42]. Class I and II HDACs contain zinc in their catalytic site and are inhibited by trichostatin A. Sirtuins instead are NAD(+) dependent deacetylases that do not contain zinc in the catalytic site and are not inhibited by trichostatin A. The seven known mammalian sirtuins differ in their subcellular localization and acetylated substrate specificity. The most studied SIRT1, as well as

SIRT6 and SIRT7 are predominantly nuclear, SIRT2 is mainly cytoplasmic and SIRT3, SIRT4 and SIRT5 are mitochondrial; the seven sirtuins were found across all the studied tissues [43, 44].

The list of SIRT2 substrates is continuously growing as research uncovers new SIRT2 biological functions. The first identified substrate was acetylated Lys40 of α-tubulin both *in vivo* and *in vitro*, and SIRT2 was reported to co-localize with the microtubule network [45]. Interestingly, α-tubulin can also be deacetylated by HDAC6 [46].

SIRT2 also regulates differentiation of various cells types for example the differentiation of adipocytes through Foxo1 (forkhead Box O1) deacetylation [47]. Interestingly, SIRT2 was shown to promote [48] as well as to inhibit [49] oligodendrocyte differentiation. In Schwann cells, SIRT2 promotes myelin formation by deacetylating partitioning defective 3 homolog (PAR-3), a regulator of cell polarity [50]. The expression of SIRT2 in mice Schwann cells is concordant with peripheral myelination. In mouse postnatal nerves, SIRT2 relative expression increases from P1 to P14 and then remains stable.

In neurodegenerative diseases such as Parkinson's disease (PD) and Huntington's disease (HD), SIRT2 inhibition shows beneficial effects. SIRT2 inhibitors rescued α-synuclein toxicity in a Parkinson's disease cellular model as well as protected cells from dopaminergic cell death *in vitro* and *in vivo* in a Drosophila PD model [51]. Moreover, Inhibition of SIRT2 in a mouse model of Parkinson's disease suggested that it might be protective against the disease because SIRT2 deacetylated Foxo3a,

activated Bim, and induced apoptosis only in mouse brains injected with a dopaminergic neurotoxin and in toxin-treated cells [52]. In two different HD mouse models, SIRT2 inhibitors were validated as potential therapeutic targets because they were able to extend survival, improve motor function and reduced the aggregation of the mutant huntingtin in their brain that is a hallmark of the disease [53].

The role of SIRT2 in cancer development is emerging. Although controversial, SIRT2 was initially reported as a tumor suppressor because of its role in cell cycle regulation. It was described that in response to stress SIRT2 released the mitotic arrest in critically damaged cells, allowing them to undergo apoptosis [54]. Recent reports show up-regulation of SIRT2 during the G_2/M transition in Saos2 cells. SIRT2 is phosphorylated during late G_2, M phase and then as the cells exit mitosis, SIRT2 levels decrease via ubiquitination and the 26S proteosomal pathway. Mitosis associated SIRT2 phosphorylation was later identified at Ser-368 by cdk1.[55, 56]. Moreover, SIRT2 is also phosphorylated at Ser-332 by CyclinE-Cdk2, CyclinA-Cdk2 and p35-Cdks and this phosphorylation inhibits SIRT2 enzymatic activity. However, experiments in HeLa and HEK293 cells with wild-type SIRT2 and SIRT2 phosphorylation mutants showed no effect on cell cycle progression or proliferation, although there was an effect on cell adhesion [57]. Additional involvement of SIRT2 in normal mitotic progression was demonstrated. SIRT2 appears to control the activity of the anaphase promoting complex/cyclosome (APC/C) by deacetylating the APC/C co-activators CDH1 and cdc20, which enhance their binding to the complex and hence prevent chromosomal instability during mitosis [58]. Further evidence of a potential role of SIRT2 as a tumor

suppressor in some tissue types is found in SIRT2 knockout mouse models that despite presenting normal development, aged SIRT2-deficient mice developed spontaneous and gender-specific tumors. The females mainly developed mammary tumors whereas the males developed hepatocellular carcinomas [58].

Conversely, the role of SIRT2 in control of cellular responses to stress and tumorigenesis led to testing of the antitumor activity of SIRT2 inhibitors. Both SIRT2 and SIRT1 emerged as attractive targets because they deacetylate major regulatory proteins, such as p53 and histone H4K16. Their inhibition with cambinol decreased viability of Burkitt lymphoma cells [59, 60]. Additionally, SIRT2 and HDAC6 deacetylate Lys104 of K-RAS that increases K-Ras transforming activity [61]. In the same line of evidence, SIRT2 was shown to stabilize Myc oncoproteins. In neuroblastomas and pancreatic cancer cells SIRT2 was upregulated and promoted cell proliferation by inhibiting the ubiquitin-protein ligase *NEDD4* gene expression. SIRT2 binds the *NEDD4* promoter repressing its activity and deacetylates Lys16 of histone H4; therefore inhibition of SIRT2 resulted in reactivation of the NEDD4 and reduced N-Myc and c-Myc expression stopping the CHP134 neuroblastoma cells and MiaPaca-2 pancreatic cancer cell proliferation [62]. Additional support to the benefit of SIRT2 inhibition in cancer is found in human gliomas. Despite that SIRT2 was reported down-regulated in several samples of human gliomas, SIRT2 activity was proven essential for survival of glioma cells [63, 64]. He et al. reported in 2012 that SIRT2 pharmacological inhibition and silencing induced both apoptosis and necrosis response of C6 glioma cells. Other cancer cells were also selectively killed by the small molecule SIRT2 inhibitor AC-

93253. In four different cancer cell lines, DU145 (prostate), MiaPaca2 (pancreas), A549 and NCI-H460 (lung) inhibition of SIRT2 was dramatically more cytotoxic than to the counterpart human control cells. Live cell imaging with HeLa cells suggested that AC-93253 induced primarily apoptosis with the presence of some necrotic cells [65]. In microglial cells, inhibition of SIRT2 with another selective small molecule SIRT2 inhibitor, AGK2, resulted in decreased BV2 microglial cells viability by inducing both necrosis and late-stage apoptosis [66]. Of note, in program necrosis, specifically when activated by death ligands such as tumor necrosis factor-alpha (TNF-α), SIRT2 was essential for the formation of the receptor-interacting protein 1 (RIP1) and receptor-interacting protein 3 (RIP3) complex in L929. Upon TNF-α stimulation, association of RIP1 with the RIP3 bound to SIRT2 can occur because SIRT2 is able to deacetylate RIP1 Lys-530 and allow a stable RIP1-RIP3 complex to proceed in the necroptotic program [67].

Despite opposing reports exhibiting a dual role of SIRT2 in both promoting and suppressing tumor formation, pharmacological inhibition of SIRT2 in age-related disorders including various types of cancer is attractive [68]. Yet, there are no highly potent and specific inhibitors for SIRT2. Specificity was not completely tested because most of the available SIRT2 inhibitors have only been screened against SIRT1 and SIRT3 and not the other sirtuins [69].

Overall, the two proposed NF2 therapeutic targets LIM domain kinases that emerged from an over-activated merlin pathway in NF2, and SIRT2 identified in an unbiased screen have been associated with tumorigenesis. Hence, both are currently

attracting the interest of pharmaceutical companies to target them for cancer therapeutics.

Figures

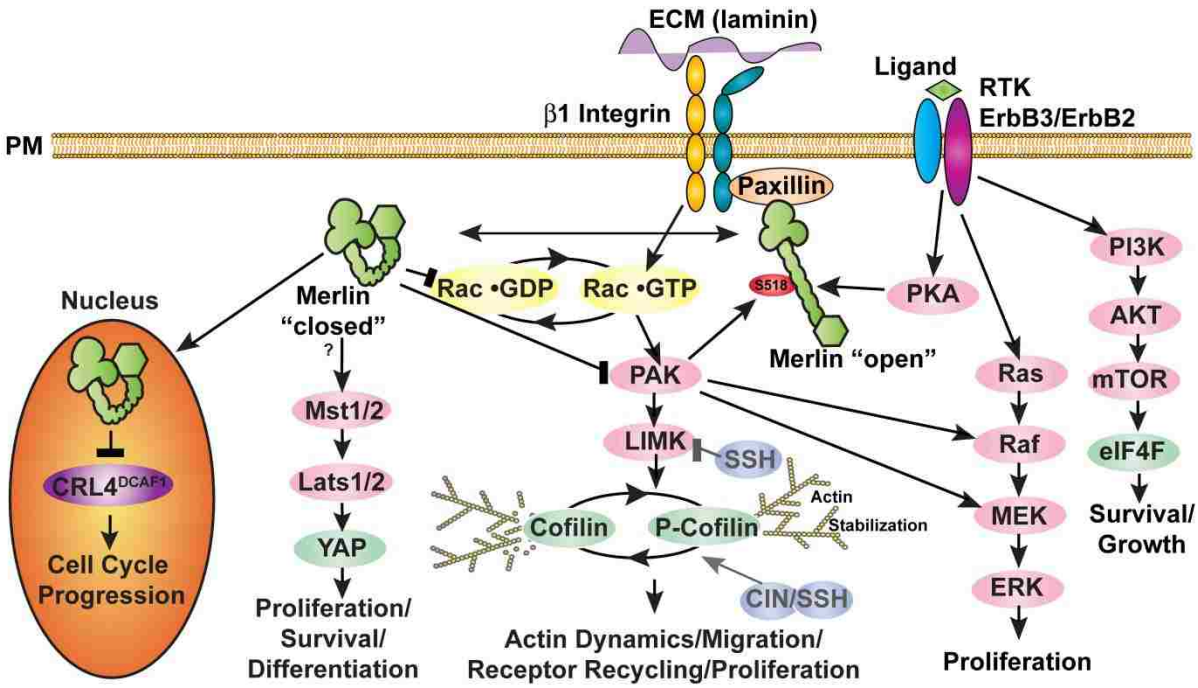

Figure 1. Merlin Signaling Pathways

Diagram summarizes the pathways modulated by merlin. Depicted are the RasGTPase, the PI3K/AKT/mTOR pathway, mitogenic receptors (e.g. EGFR, ErbB2), extracellular matrix receptors (β1 integrins), nuclear ubiquitination cascades, and the most recently-described Mst-YAP pathway. Diagram by Dr. Fernandez-Valle.

CHAPTER TWO: LIM DOMAIN KINASES AS POTENTIAL THERAPEUTIC TARGETS FOR NEUROFIBROMATOSIS TYPE 2

Introduction

Mutations in the tumor suppressor gene *NF2* cause neurofibromatosis type 2 (NF2), an autosomal dominant disorder with an incidence of about one in 25,000 individuals [4]. The characteristic feature of NF2 is the development of bilateral vestibular schwannomas that typically cause deafness, facial paralysis and disequilibrium following surgical removal to prevent life-threatening complications. Frequently, NF2 patients also develop multiple schwannomas in other nerves as well as meningiomas and ependymomas [1]. Mutations in the *NF2* gene are also common in malignant mesothelioma [70]. Currently, the standard treatment for NF2 schwannomas is microsurgery or stereotactic radiosurgery. Unfortunately, limited operability, poor preservation of hearing, diminished functionality of facial nerves and the small risk of radiation-induced malignant transformation later, compromise good clinical outcomes. Only a handful of NF2 pre-clinical and clinical trials are ongoing, all of which utilize existing anti-cancer drugs [9, 71].

The *NF2* gene encodes a tumor suppressor called merlin or schwannomin. Merlin regulates a number of processes in Schwann cells (SCs) [7, 72]. Normal SCs usually proliferate slowly and adopt a bipolar morphology, however, merlin-deficient human schwannoma cells exhibit abnormalities in proliferation, motility and morphology in vitro [73]. Merlin's mechanism of action remains poorly understood, but appears to involve regulation of surface receptor activity and turnover by modulation of their

interactions with the actin cytoskeleton and transduction of downstream signals [7]. A potential pathway through which merlin regulates the actin cytoskeleton involves Cdc42/Rac-PAK-LIMK-cofilin [13, 74, 75]. Loss of merlin function is associated with elevated levels of active Rac and p21-activated kinase (PAK), suggesting that merlin is a negative regulator of Rac and PAK-dependent pathways. Conversely, PAK phosphorylates and inactivates merlin's tumor suppressor activity [12, 76]. Work from our laboratory has shown that activation of β1-integrin in normal SCs promotes PAK-dependent phosphorylation of merlin at serine-518 [8]. While PAK has been studied as a potential therapeutic target for NF2, its large number of substrates confounds its usefulness [15].

The LIM kinase (LIMK) family has two members, LIMK1 and LIMK2, which can be phosphorylated by Cdc42/Rac-PAK1, 2 and 4 at threonine-505/508 and converted into active serine/threonine kinases. LIMKs are also regulated by Rho-associated kinases (ROCK) and the myotonic dystrophy kinase-related Cdc42-binding kinase (MRCK). The major LIMK substrate is the actin depolymerizing and severing protein cofilin/ADF [17]. LIMK-dependent phosphorylation of cofilin at serine-3 inactivates cofilin and promotes stabilization of the actin cytoskeleton [21]. LIMKs also translocate from the cortical cytoplasm and focal adhesions, where they modulate cell morphology and motility, to the centrosome and nucleus, where they regulate mitosis and cytokinesis [16, 28, 29, 77-80]. LIMKs interact with Aurora A, a serine/threonine kinase involved in centrosome dynamics, spindle assembly and chromosome alignment and segregation during mitosis [31, 32]. Aurora A is found on duplicated centrosomes and

mitotic spindle microtubules. During early mitosis phospho-LIMKs co-localize with γ-tubulin in the centrosomes. In metaphase LIMK1 is found at the spindle poles and later redistributes to the cleavage furrow. LIMK2 is located along the spindle and at the cleavage furrow of post-mitotic cells. LIMK1 is a substrate for, and phosphorylates Aurora A to promote its autophosphorylation at Thr288 [24]. LIMK2 is an Aurora A substrate and stabilizes it by kinase and scaffolding actions [25]. LIMKs are overexpressed and implicated in various cancers, such as breast, lung, skin, liver and prostate, and several tumor cell lines [36-39]. Hence, LIMKs are emerging cancer targets yet, few inhibitors have been identified [17].

We show that the levels of total and phosphorylated LIMK and its phosphorylated substrate are elevated in sporadic vestibular schwannomas (VS) compared to normal human SCs. Utilizing *Nf2*$^{\Delta Ex2}$ mouse Schwann cells (MSCs) as a cellular model of NF2, we show that pharmacological inhibition or genetic silencing of LIMK significantly reduces proliferation of *Nf2*$^{\Delta Ex2}$ MSCs, but does not substantially affect control *Nf2*$^{flox2/flox2}$ MSCs. The decreased proliferation is due to cell cycle arrest in the G_2/M phase. Pharmacological inhibition of LIMKs with BMS-5 slows mitotic progression by decreasing phosphorylation of cofilin and Aurora A. These studies suggest that LIMKs are potential therapeutic targets for NF2 and other merlin-deficient tumors.

Materials and Methods

Inhibitors

LIMK1/2 inhibitor, BMS-5 (CAS name N-(5-(192,6-dichlorophenyl)-3-(difluoromethyl)-1H-pyrazol-5-yl)thiazol-2-yl)isobutyramide) was from SynKinase (Shanghai, China). Rapamycin and staurosporine were from Santa Cruz Biotechnology (Santa Cruz, CA, USA).

Antibodies

Antibodies used were purchased from the following sources: phospho-Cofilin Ser3 (77G2), Merlin (D1D8), phospho-LIMK1(Thr508)/LIMK2(Thr505) (used in cell lines), LIMK1, phospho-Histone3(Ser10) (D2C8), α-Tubulin (DM1A), phospho-AuroraA(Thr288)(D13A11) and β-Actin (8H10D10) from Cell Signaling (Danvers, MA, USA); LIMK1 (clone42) mouse monoclonal antibody from BD Biosciences (San Jose, CA, USA); LIMK2, phospho-LIMK1 (pThr-508), and phospho-LIMK2 (pThr-505) rabbit antibodies from Sigma-Aldrich (St. Louis, MO, USA); S-100 rabbit antibody from Dako Cytomation (Glostrup, Denmark); Cofilin rabbit antibody from Novus Biologicals (Littleton, CO, USA);Centrin-1 rabbit antibody from Abcam (Cambridge, MA, USA); Aurora A rabbit antibody from Bethyl Laboratories (Montgomery, TX, USA); Peroxidase-conjugated goat anti-rabbit-IgG from Pierce, Thermo Fisher Scientific (Rockford, IL, USA); Highly cross-adsorbed Alexa Fluor® 488 goat anti-rabbit IgG (H+L) antibody from Invitrogen (Grand Island, NY, USA).

Generation of $Nf2^{\Delta Ex2}$ MSCs

$Nf2^{\Delta Ex2}$ MSCs were generated in vitro by transducing *$Nf2^{flox2/flox2}$* Schwann cells with an Adeno-Cre virus (University of Iowa Gene Transfer Vector Core) as previously described [81]. The *$Nf2^{\Delta Ex2}$* MSCs were used up to passage 20. All protocols are in accordance with guidelines of and approved by the AAALAC International-certified UCF Institutional Animal Care and Use Committee.

Human Schwann Cell Cultures

Vials of frozen purified human SCs received from Dr. Patrick Wood at the University of Miami School of Medicine (Miami, FL, USA) were thawed and cultured on Corning dishes coated with 200 µg/ml poly-L-lysine (PLL) hydrobromide (Sigma-Aldrich) and 50 µg/ml Laminin (Invitrogen) containing D10M growth media: DMEM (Gibco) plus 10% heat inactivated fetal bovine serum (HIFBS) (HyClone, Logan, UT, USA), 2 µM Forskolin (Sigma), 0.02 mg/ml Pituitary Extract (Biomedical Tech. Inc) and 1% Penicillin/Streptomycin (Gibco). Frozen vials from the stock bank of HSC were prepared by the Life Alliance Organ Recovery Agency at the University of Miami School of Medicine and cannot be traced to the specific donor. HSC were prepared from 10 cm biopsy of sural nerve/cauda equine from cadaveric adult human donors. Nerve fragments were incubated several days, dissociated and plated. SCs were purified by immunopanning with NGFR p75 antibodies. Culture purity based on S100 immunostaining was 96-99%. HEI-193 cells were purchased from ATCC (Manassas, VA, USA) and grown in DMEM plus 10% HIFBS and 1% Penicillin/Streptomycin.

Human Schwannoma Samples

Frozen specimens of human sporadic vestibular schwannomas with different types of *NF2* mutations were procured with patient informed consents at The Ohio State University according to Institutional Review Board regulations.

Western Blot Analysis

Cultured cells were lysed in modified RIPA buffer (25 mM Tris-HCl pH 7.6; 150 mM NaCl: 1% Triton X-100, 1% Sodium dodecyl sulfate with protease inhibitor cocktail and phosphatase inhibitor cocktails 2 and 3, Sigma-Aldrich). VS specimens (0.1–0.2 gr) were homogenated in 900 µl of modified RIPA buffer with 25–30 strokes in a Wheaton Micro Tissue Grinder glass set # 528 (Wheaton Scientific, Millville, NJ, USA) on ice. Lysates were rotated for 10 min at 4°C and centrifuged for 10 min at 4°C, 15,000 rpm. Protein concentration was determined by DC Assay (BioRad, Hercules, CA, USA), and 10–20 µg of protein in Laemmli buffer was resolved in 10% or 4–20% polyacrylamide gels (Pierce/Fisher Scientific), transferred to PVDF membrane (Immobilon-P, Millipore, Bedford, MA) and analyzed by western blotting with anti-LIMK1, (1:500) from BD for human samples and (1:500) from Cell Signaling for mouse samples, LIMK2 (1:500), P-cofilin-Ser3 (1:1,500), cofilin (1:70,000), merlin (1:500), S-100 (1:300), P-LIMK1-Thr508 (1:1,000), P-LIMK2-Thr505 (1:1,000), P-LIMK1(Thr508)/LIMK2(Thr505) (1:200) used in mouse and HEI193 cell lines, P-Aurora (1:1,000), AuroraA (1:500) and β-Actin (1:15,000) followed by corresponding secondary antibodies (1:20 000). Western blots

were quantified by densitometry using NIH ImageJ software. Intensities were normalized to β-actin loading controls.

LIMK1 and LIMK2 Knockdown in $Nf2^{\Delta Ex2}$ MSCs

$Nf2^{\Delta Ex2}$ MSCs were plated onto PLL-coated (200 µg/ml) 6-well dishes, cultured at 37ºC, 7% CO2, in medium containing DMEM/F12 (Invitrogen/Life Technologies, Grand Island, NY, USA) plus N2 supplement (Invitrogen: Burlington, ONT, Canada) and 1% Penicillin/Streptomycin . When cultures reached 40% confluence, lentiviral transduction particles were added at 5 multiplicity of infection (MOI) in growth medium plus 8 µg/ml hexadimethrine bromide (Sigma). MISSION shRNA lentiviral particles for mouse gene silencing were from Sigma-Aldrich. LIMK1 clone IDs: NM_010717.1-1546s1c1 (named construct #44); NM_010717.1-1414s1c1 (#47) and LIMK2 clone IDs: NM_010718.1-1409s1c1 (#73); NM_010718.3-827s21c1 (#95). Negative control was pLKO.1-puro non-mammalian shRNA (SHC002V). Optimum MOI determined empirically with pLKO.1-puro-CMV-TurboGFP transduction lentiviral particles (SHC003V) titer. After 18–20 hours, infection medium was replaced with fresh medium for 24 hours and subsequently replaced with growth medium containing 1µg/ml puromycin (Sigma-Aldrich) to select transduced cells. The puromycin concentration was determined performing a toxicity curve.

Reintroduction of NF2 into $Nf2^{\Delta Ex2}$ MSCs

To reintroduce merlin into *$Nf2^{\Delta Ex2}$* MSCs, 1.5–2 million cells were resuspended in 100 µl of basic Nucleofector solution for mammalian glial cells with supplements (Lonza,

Cologne, Germany) plus 1 µg of pFC15K HaloTagCMVd1-NF2 using an Amaxa Nucleofector II device and Program A-033. 1 ml of warm growth medium was added and 50 µl of cell suspension was seeded on coated 11mm round German glass coverslips (Carolina Biol., Burlington, NC, USA) containing 100 µl of equilibrated growth medium and incubated 40 hours at 37°C, 7% CO2 before analysis.

Immunofluorescence

Cells were plated on coated German glass coverslips and immunostained as previously described [81]. Labeling of Halo-Tag-*NF2*-transfected cells was done in vivo with HaloTag® TMR Ligand (Promega, Madison, WI, USA) following manufacturer's rapid labeling protocol. Confocal images were acquired with a Zeiss LSM710 microscope with 3 spectral detection channels, 5 laser lines - 458, 488, 514,543 & 633 nm, FL filter set 49 DAPI, EX G365 shift free, FL filter set 43 CY 3 shift free, FL filter set 38 Endow GFP, shift free, Plan-Apochromat 63x/1.40 Oil DIC M27 and EC Plan-Neofluar 40x/1.3 DIC WD=0.21 M27 objective lenses on an AxioObserver Z1 Stand and ZEN2009 software. Fluorescence was collected from a single plane on separate channels maintaining the same acquisition parameters for each labeled protein. Images from each experiment were processed identically with ZEN2011 software. For spindle images, Z-stacks were collected with the 63xOil objective and 3.5 zoom factor. 2-D images were obtained by median filter and maximum intensity projection with ZEN2011.

Cell Viability Assay

Cell viability was assessed by CellTiter-Fluor assay (Promega) following manufacturer's specifications. Cells were seeded in 384-well format, centrifuged 1 min at 500 rpm and incubated at 37ºC, 7% CO2. After cell attachment (2.5–3.5 hrs), 5 µl/well of compound/vehicle solution was added and plates were quick spinned and incubated for 24 hrs. Fluorescence was measured with a Synergy H1 Hybrid plate reader (BioTek, Winooski, VT, USA).

Caspase Activity Assay

Caspase activity was assessed by the Apo-ONE homogeneous Caspase-3/7 assay (Promega) following manufacturer's specifications. Fluorescence was measured with a plate reader.

Membrane Asymmetry Assay

Cell membrane asymmetry was measured with the Violet Ratiometric Membrane Asymmetry Probe/Dead Cell Apoptosis Kit (Invitrogen/Life Technologies). Cells were seeded in 200 µg/ml PLL-coated 6-well plates and incubated with BMS-5/vehicle for 24 hrs. Cell were harvested and assayed following manufacturer's instructions. Samples were analyzed on a BD Canto-II (Becton, Dickinson and Co, Franklin Lakes, NJ, USA) flow cytometer setting excitation and collection emission wavelength recommended by the manufacturer. The ratio parameter was established using BD FACSDiva™ 6.1.3 software as recommended by the manufacturer.

Proliferation Assays

Cell proliferation was studied with two different techniques. *Nf2*$^{\Delta Ex2}$ MSCs seeded in a 24-well format, had cell numbers assessed with the Crystal Violet Assay as previously described [82]. Absorbance at 595 nm was measured with a µQuant plate reader (BioTek).

Rate of DNA synthesis was evaluated at 24 hrs with the Click-iT EdU Microplate Assay (Invitrogen/ Life Technologies). The assay was carried out in 96- and 384-well plate formats following manufacturer's instructions without the Amplex® UltraRed amplification steps. DAPI stain was included in the wash after the reaction cocktail incubation step. Oregon green-488 and DAPI fluorescence was quantified by a plate reader.

Cell Cycle Analysis

The cell cycle was analyzed by flow cytometry with propidium iodine (PI) staining and BrdU/7AAD. 10^6 ethanol fixed cells were PI stained using 500 µl PI/RNase staining buffer (Beckton-Dickinson). Samples were examined on a BD Canto-II flow cytometer and histograms were analyzed using ModFit LT software (Verity Software House, Topsham, ME, USA). For each sample, 10,000 events were collected.

The BrdU/7AAD assay kit was from Beckton-Dickinson. Cells were seeded in 6-well plates and treated with inhibitor/vehicle overnight. Next day, cultures were incubated with 10 µM BrdU for 3 hrs, and the assay performed according to manufacturer's instruction. Samples were analyzed with a BD Canto-II flow cytometer

using the BD FACSDiva™ 6.1.3 software. FlowJo software (Tree Star, Inc, Ashland, OR, USA) was used for analysis of acquired data.

Statistical Analysis

GraphPad Prism version 5.0 for Windows (GraphPad, La Jolla, CA, USA) was used for statistical analysis and graph generation of experimental data from three independent experiments. Dose response experiments were analyzed by non-linear regression (four parameters). Statistical analysis is indicated for each experiment.

Results

LIMK and Phospho-Cofilin Levels are Elevated in $Nf2^{\Delta Ex2}$ MSCs Compared to Controls

Using two complementary techniques, we assessed the levels of LIMK and phospho-Ser3-cofilin in *Nf2*-deficient ($Nf2^{\Delta Ex2}$) MSC lines developed by in vitro ad-Cre deletion of *Nf2* exon2 from $Nf2^{flox2/flox2}$ MSCs [83]. By immunostaining $Nf2^{\Delta Ex2}$ MSCs were confirmed to be merlin-deficient and expressed the SC marker S100 (Figure 2a). Merlin-deficient Schwann cells were larger than control $Nf2^{flox2/flox2}$ MSCs and had increased levels of F-actin revealed by phalloidin staining. The intensity of LIMK1 and LIMK2 immunofluorescence was higher in $Nf2^{\Delta Ex2}$ MSCs than in controls and was detected throughout the cell. Consistent with increased LIMK activity, the intensity of phospho-Ser3-cofilin immunofluorescence was also higher in $Nf2^{\Delta Ex2}$ MSCs than in controls (Figure 2 a, b).

We also assessed merlin expression in control *Nf2*$^{flox2/flox2}$ and *Nf2*$^{\Delta Ex2}$ MSCs by western blotting using an N-terminal merlin antibody. Merlin was detected in *Nf2*$^{flox2/flox2}$ MSCs but not in *Nf2*$^{\Delta Ex2}$ MSCs (Figure 2 c). The status of the *Nf2* gene was also confirmed by PCR analysis of DNA and revealed deletion of exon 2 in *Nf2*$^{\Delta Ex2}$ as evidenced by a 338-bp band (Figure 2 d) [83].

In addition, western blotting confirmed that levels of both LIMK1 and LIMK2 protein were higher in *Nf2*$^{\Delta Ex2}$ MSCs than in *Nf2*$^{flox2/flox2}$ MSCs (Figure 2 e). We detected a coordinate increase in the level of phospho-Ser3-cofilin in *Nf2*$^{\Delta Ex2}$ MSCs with respect to control consistent with high levels of LIMK activity (Figure 2 f).

Reintroduction of Wild-type NF2 Normalizes LIMK Protein Levels

To assess whether elevated LIMK levels were linked to merlin inactivation, we reintroduced a halo-tagged wild-type human *NF2* into *Nf2*$^{\Delta Ex2}$ MSCs by nucleofection. This method yielded ~10% transfection rate, determined by halo-tag fluorescence labeling. Re-expression of merlin in cultured *Nf2*$^{\Delta Ex2}$ MSCs generally decreased LIMK1, LIMK2 and phospho-Ser3-cofilin levels (Figure 3 a, b). This result supports a relationship between merlin inactivation and increased LIMK expression and activity.

Pharmacological Inhibition of LIMK1/2 by BMS-5 or Genetic Silencing of LIMK1/2 Reduces Nf2$^{\Delta Ex2}$ *MSC Viability*

We next sought to determine whether LIMK was a potential drug target for NF2. We tested the efficacy of BMS-5, a highly selective small molecule inhibitor of LIMK1/2, on reducing phosphorylation of cofilin on Ser3 [84]. BMS-5 inhibited cofilin-Ser3

phosphorylation in a dose-dependent manner in *Nf2*$^{\Delta Ex2}$ MSCs with an IC_{50} of ~ 2 µM (Figure 4 a, b). We next tested the ability of BMS-5 to reduce viability of *Nf2*$^{\Delta Ex2}$ MSCs. The 100% viability control was 0.1% DMSO and a positive cell death control was obtained with 50 µM rapamycin (RM) that caused approximately 80% cell death in 24 hours. BMS-5 reduced *Nf2*$^{\Delta Ex2}$ MSC viability in a dose-dependent manner with an IC_{50} of 3.9 µM (Figure 4 c), but did not significantly reduce the viability of control *Nf2*$^{flox2/flox2}$ MSCs at equivalent BMS-5 concentrations (Figure 4 d). At 10µM BMS-5, *Nf2*$^{\Delta Ex2}$ MSC viability was 40% compared to 83% for controls.

To confirm the validity of LIMK as a drug target, we knocked down LIMK1 and LIMK2 in *Nf2*$^{\Delta Ex2}$ MSCs using lentiviral shRNA transduction (Supplementary Figure 1). Consistent with the BMS-5 results, LIMK1 and LIMK2 knockdown reduced viability of *Nf2*$^{\Delta Ex2}$ MSCs compared to scrambled shRNA controls in a 24 hour assay (Figure 4 e). These results suggest that LIMK inhibition or silencing in merlin-deficient cells reduces their viability either by promoting cell death or hindering proliferation.

Decreased Viability of Nf2$^{\Delta Ex2}$ *MSCs in Response to BMS-5 or LIMK Silencing is Independent of Apoptosis.*

To determine if BMS-5 promoted *Nf2*$^{\Delta Ex2}$ MSCs apoptosis, we measured caspase 3/7 activity. We found that BMS-5 did not activate caspase3/7, whereas the positive control, staurosporine, promoted dose-dependent activation of caspase 3/7 (Figure 5 a). To determine if BMS-5 promoted caspase-independent apoptosis, we analyzed BMS-5-treated *Nf2*$^{\Delta Ex2}$ MSCs by flow cytometry using a ratiometric membrane asymmetry probe that detects loss of membrane phospholipid asymmetry associated

with apoptosis. We observed only a small increase (3.5%) of apoptotic cells after 7 hours of BMS-5 treatment (Figure 5 b). Consistent with pharmacological LIMK inhibition, knockdown of LIMK1 or LIMK2 was not associated with caspase 3/7 activity increase compared to scrambled shRNA controls examined 24 hours after plating (Figure 5 c). Similarly, caspase-independent apoptosis was not observed in *Nf2*$^{\Delta Ex2}$ MSCs transduced with either LIMK1 or LIMK2 shRNA (Figure 5 d). These results suggest that pharmacological inhibition and genetic silencing of LIMK affect *Nf2*$^{\Delta Ex2}$ MSC viability through an apoptosis-independent mechanism.

Pharmacological Inhibition of LIMK1/2 by BMS-5 Reduces DNA Synthesis and Cell-Cycle Progression

We next assessed the ability of BMS-5 to interfere with proliferation of *Nf2*$^{\Delta Ex2}$ MSCs. The cells were incubated with 1 and 2 µM BMS-5 for 24, 48 and 72 hours and cell numbers were measured using crystal violet staining. We observed fewer BMS-5 treated *Nf2*$^{\Delta Ex2}$ MSCs than DMSO-treated controls (Figure 6 a). In addition, we found that BMS-5 decreased DNA synthesis in *Nf2*$^{\Delta Ex2}$ MSCs in a dose-dependent manner (Figure 6 b).

To test the possibility that the decrease in proliferation was a consequence of cell-cycle inhibition, we performed flow cytometry analysis of cells stained with propidium iodine (PI). BMS-5 interfered with *Nf2*$^{\Delta Ex2}$ MSCs cell-cycle progression as evidenced by an increase in the percentage of diploid cells trapped in the G_2/M phase (Figure 7 a). We further analyzed the distribution of cells among the cell-cycle phases using a BrdU/7AAD assay. There was a significant increase in the number of cells

accumulating in the G_2/M phase in samples treated with 5 μM BMS-5 as compared to vehicle control (20% vs. 42%). This was accompanied by a decrease in the number of BMS-5 treated cells in G_1 as compared to control (41% vs. 26%). This is consistent with the results obtained by analysis of PI staining (Figure 7 b-c). Overlay of the 7AAD-area histograms clearly demonstrated a significant increase in the G_2/M population in BMS-5 compared to DMSO treated cells (Figure 7 d). Furthermore, the increase in the G_2/M population was accompanied by an increase in the number of cells with higher DNA content consistent with a polyploidy or multinucleated cell population. There was also a smaller but substantial change in number of cells detected in the S-phase of cell cycle in samples treated with BMS-5 as compared to DMSO control. Lastly, the population of cells in the S phase decreased with increasing BMS-5 concentration (Supplementary Figure 2). These results taken together suggest that inhibition of LIMK activity in *Nf2*$^{\Delta Ex2}$ MSCs interferes with progression of the G_2/M phase of the cell cycle, thereby decreasing the number of viable *Nf2*$^{\Delta Ex2}$ MSCs.

BMS-5 Inhibition of LIMK1/2 Activity Decreases Aurora A Phosphorylation and Causes Formation of Abnormal Mitotic Spindles

To identify additional down-stream effects of BMS-5 (beyond inhibition of cofilin-Ser3 phosphorylation) that could cause a G_2/M arrest, we tested the levels of Aurora A phosphorylation. Aurora A interacts with both LIMK1 and 2 and is a major regulator of mitotic spindle assembly and chromosomal alignment and segregation. We found that *Nf2*$^{\Delta Ex2}$ MSCs treated with increasing concentrations of BMS-5 had a dose dependent decrease in phosphorylation of Aurora A at Thr288 (Figure 8 a, b).

We next studied the effect of BMS-5 on the spindle assembly visualizing the mitotic nuclei and spindle machinery by immunostaining. We found that *Nf2*$^{\Delta Ex2}$ MSCs had normal spindle assembly and BMS-5 treated *Nf2*$^{\Delta Ex2}$ MSCs showed abnormal spindle structure (Figure 9 a). Analyzing the centrosome positioning by immunostaining for centrin-1, we found that BMS-5 treated cells were not able to organize the centrosomes and generally had more than two with different sizes (Figure 9 b). We conducted cell cycle analysis and found that the percentage of cells in late G_2/M, visualized by positive immunostaining for the mitotic marker phospho-Ser10-histone3 (pH3), significantly increased from 5% to 17% in the BMS-5 treated *Nf2*$^{\Delta Ex2}$ MSCs compared to DMSO controls (Figure 9 c, d). We observed a highly significant decrease in the percentage BMS-5 treated *Nf2*$^{\Delta Ex2}$ MSCs that advanced to late mitotic phases (anaphase/telophase). Moreover, BMS-5 treated *Nf2*$^{\Delta Ex2}$ MSCs had abnormal spindles and chromosomes did not align at the center as occurs in metaphase (Figure 9 a-e). These results suggest that LIMK inhibition exerts its anti-proliferative effect not only by altering organization of the actin cytoskeleton through inhibition of cofilin phosphorylation but also by decreasing LIMK dependent activation of Aurora A.

LIMKs Levels are Elevated in Representative Samples of Human Vestibular Schwannoma Compared to Human SCs

To examine the relevance of LIMK inhibition to NF2, we compared LIMK1 and LIMK2 protein and phosphorylation levels in a small number of samples of HSCs from normal individuals and sporadic human vestibular schwannomas (VSs). We observed a significant increase ($P<0.05$ determined using unpaired t-test of HSC vs. VS

populations, two-tailed) in both the protein and phospho-Thre508 levels of LIMK1 in VSs compared to HSCs (Figure 10 a, b). Similarly, both LIMK2 and phospho-Thr505-LIMK2 levels showed a tendency to be higher in VSs compared to HSCs (Figure 10 c, d). Interestingly, the proportion of phospho-Ser3-cofilin to the total cofilin was higher in VSs than in HSCs (Figure 10 e).

We also measured LIMK protein and phosphorylation levels in a human schwannoma cell line, HEI-193, developed from a NF2 patient by immortalization with HPV E6-E7 genes [85]. Although the phospho-Thr508/Thr505 LIMK1/2 antibody recognized multiple bands, the relative intensities of the most prominent phospho-LIMK 1/2 (Thr508/Thr505) bands were also higher in HEI-193 cells than in control HSCs (Figure 10 f).

Discussion

LIMK Expression and Activity are Elevated in Merlin-deficient SCs Compared to Normal SCs

Here we document an association between loss of merlin function and increased levels of LIMK1 and LIMK2 expression and activity. The increased LIMK activity in *Nf2*-deficient MSCs is consistent with its activation by Cdc42/Rac-PAK1, 2 and 4 [17], which have been well-documented to be increased in schwannomas [12, 15]. Importantly, reintroduction of merlin into $Nf2^{\Delta Ex2}$ MSCs reduced LIMK and phospho-Ser3-cofilin levels, further supporting an association between loss of merlin function and inactivation of cofilin's actin-severing and depolymerizing activity downstream of activation of the Rac/PAK/LIMK pathway. In agreement with previous studies of human schwannoma

cells, we found that *Nf2*$^{\Delta Ex2}$ MSCs exhibited an abnormal actin cytoskeleton compared to control MSCs [73]. Interestingly, similar cytoskeleton characteristics, indicative of F-actin stabilization, have been reported in C2C12 and HeLa cells overexpressing LIMK [21, 86]. We propose that phosphorylation and inactivation of cofilin downstream of elevated Rac/PAK/LIMK activity could account for the reported increased cell size and abundance of actin filaments observed in *Nf2*$^{\Delta Ex2}$ MSCs and human schwannoma cells [87].

Inhibition of LIMK Activities Causes Cell-Cycle Arrest of Nf2$^{\Delta Ex2}$ MSCs by Preventing Aurora A Activation

We recently demonstrated using BMS-5 that LIMK-dependent phosphorylation of cofilin is necessary for stable alignment of SC processes along sensory neuron axons in culture [88]. Here we showed that BMS-5 decreased *Nf2*-deficient MSCs viability in a dose-dependent manner while having little effect on controls. These results suggest a potential therapeutic window for treatment of schwannomas with LIMK inhibitors. Studies using shRNA knockdown of LIMK1 and LIMK2 in *Nf2*$^{\Delta Ex2}$ MSCs confirmed the specificity of BMS-5 on LIMK activity. Intriguingly, during LIMK silencing in *Nf2*$^{\Delta Ex2}$ MSCs, we found that these cells did not sustain long-term LIMK knockdown and were able to restore their original expression levels. Thus, we only used cells within their first two passages after puromycin selection. We speculate that *Nf2*$^{\Delta Ex2}$ MSCs silence LIMK shRNA by a methylation-dependent mechanism as shown for PAK shRNAs in schwannoma cells [15].

Inhibition of LIMK activity with BMS-5 reduced *Nf2*$^{\Delta Ex2}$ MSCs viability by causing their arrest at the M phase of the cell cycle. Others have shown that LIMK's localization and activity changes during the cell cycle and that cofilin phosphorylation dynamics are necessary for successful cytokinesis [28, 29, 79]. Importantly, LIMK1 knockdown in HeLa cells or treatment with a LIMK inhibitor peptide resulted in delayed mitotic progression and irregular spindle orientation [78]. These reports support our conclusion that inhibition of LIMK activity with BMS-5 arrested *Nf2*-deficient cells in the M phase thereby decreasing the number of cells in S phase, and increasing the number of polyploid cells.

The reported interaction and functional cooperation of LIMK1 and 2 with Aurora A led us to explore the effect of LIMK inhibition with BMS-5 on Aurora A autophosphorylation [32]. In agreement with the observations made with LIMK1 knockdown in PC-3 cells, we found that BMS-5 reduced Aurora A phosphorylation at Thr288 [24]. It is important to note that BMS-5 does not directly inhibit Aurora A kinase activity, because BMS-5 (compound 3 in ref.[84]) was tested in vitro against a panel of kinases and Aurora A retained 100% activity when tested with 10 µM BMS-5 [84]. Interestingly, the abnormal spindle and centrosome organization observed here resembles the abnormal metaphase spindles with multipolar and/or wheel-barrel shape and non-assembled chromosomes observed in a LIMK2 knockdown in SH-EP neuroblastoma cells [79]. The integrity of the mitotic spindle is required for progression from metaphase to anaphase, and any abnormality in the spindle assembly checkpoint delays or hinders the onset of anaphase. Hence, inhibition of LIMKs activity by BMS-5

leads to inhibition of Aurora A kinase activity, and thus provides a molecular pathway for the G_2/M block of merlin deficient SCs treated with BMS-5.

Recently, LIMK has been show to promote tumor neovascularization through the VEGF/p38/MK2/LIMK1/annexin1 pathway [89]. This finding may potentially connect LIMK inhibition with the observed reduction in angiogenesis *in vivo* following treatment with Bevacizumab, which reduces tumor volumes and, in some patients, restores some hearing [90]. Thus, we speculate that inhibition of LIMK might halt tumor progression not only by interfering with cell-cycle progression in schwannoma cells, but also by inhibiting angiogenesis.

In conclusion, our studies suggest a potential therapeutic target for NF2, the LIMKs, which are recognized substrates of Cdc42/Rac-PAK1,2,4. We show enhanced LIMK expression and activity in merlin-deficient MSCs and as well as VS as opposed to controls. Reduction in LIMK activity or protein levels decreases *Nf2*-deficient MSC viability by arresting cells in the prometaphase stage of the cell-cycle in association with decreased activation of Aurora A necessary for centrosome and mitotic spindle organization. Future studies addressing whether LIMK inhibition is an effective treatment for schwannomas in mouse models of NF2 are warranted.

Figures

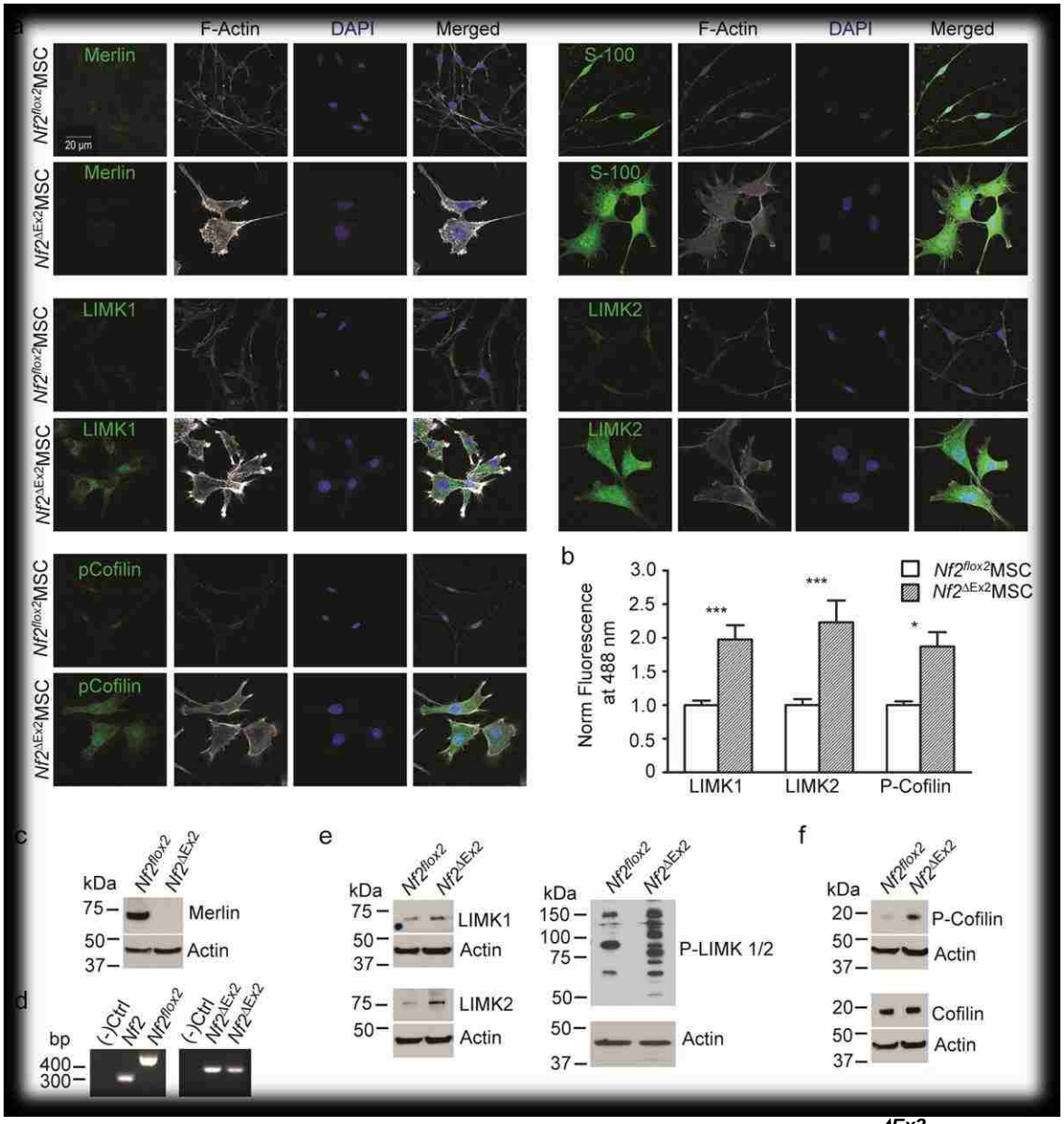

Figure 2. Elevated Levels of LIMK and Phospho-Ser3-Cofilin in *Nf2$^{\Delta Ex2}$* MSCs Compared to Control MSCs.

(a) Representative confocal images of *Nf2$^{\Delta Ex2}$* MSCs and *Nf2$^{flox2/flox2}$* MSCs grown overnight on glass coverslips, fixed and immunostained with the indicated antibodies (green). F-actin was visualized with phaloidin-Alexa633 (white) and the nucleus was visualized by DAPI stain (blue). Scale bar: 20 µm. **(b)** Quantitation of the immunofluorescence for the indicated proteins in three independent experiments was performed with Volocity software. ***P<0.001; *P<0.05

determined by two-way ANOVA using Bonferroni post-tests. **(c)** Characterization of *Nf2*$^{flox2/flox2}$ and *Nf2*$^{\Delta Ex2}$ MSCs. Control *Nf2* with the exon2 flanked by loxP sites, *Nf2*$^{flox2/flox2}$ and *Nf2*$^{\Delta Ex2}$ MSCs analyzed by western blotting for N-terminus merlin and **(d)** PCR analysis of genomic DNA. Primers P4/P5 amplified a 305-bp band for wild type *Nf2* FVB/N and a 442-bp band for *Nf2*$^{flox2/flox2}$ and primers P6/P5 amplified a 338-bp band for *Nf2*$^{\Delta Ex2}$. **(e)** *Nf2*$^{\Delta Ex2}$ MSCs and control *Nf2*$^{flox2/flox2}$ MSCs analyzed by western blotting for LIMK1, LIMK2, phospho-LIMK1/2 (Thr508/505), and **(f)** phospho-Ser3-cofilin and cofilin. Anti-β-actin was used as a loading control.

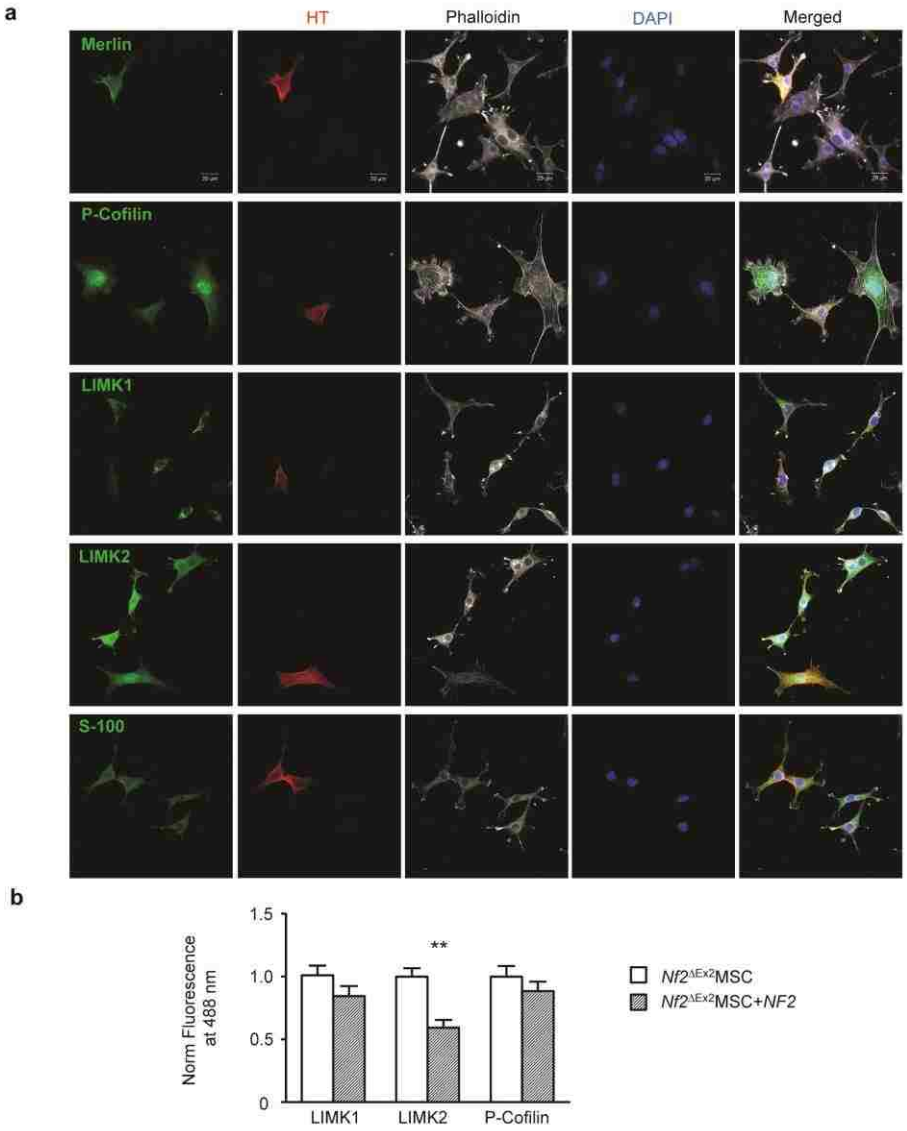

Figure 3. Reintroduction of Wild-type Merlin Normalizes LIMK Expression Levels.

(a) *Nf2*$^{\Delta Ex2}$ MSCs were transfected with Halo-tag-*NF2* and incubated for 40 hrs on glass coverslips coated with 200 μg/ml PLL and 10 μg/ml Laminin. Transfected cells were identified by halo-tag TMR labeling (red). Cells were fixed and immunostained for the indicated proteins (green). F-actin was visualized with phaloidin-Alexa633 (white) and the nucleus with DAPI (blue). Confocal images are representative of three independent experiments. Scale bar: 20 μm. **(b)** Quantitation of (a). Measurements of the mean pixel intensity fluorescence in the green channel of 2 experiments for the indicated proteins were performed with Volocity software. **P*<0.05 determined by two-way ANOVA using Bonferroni post-tests.

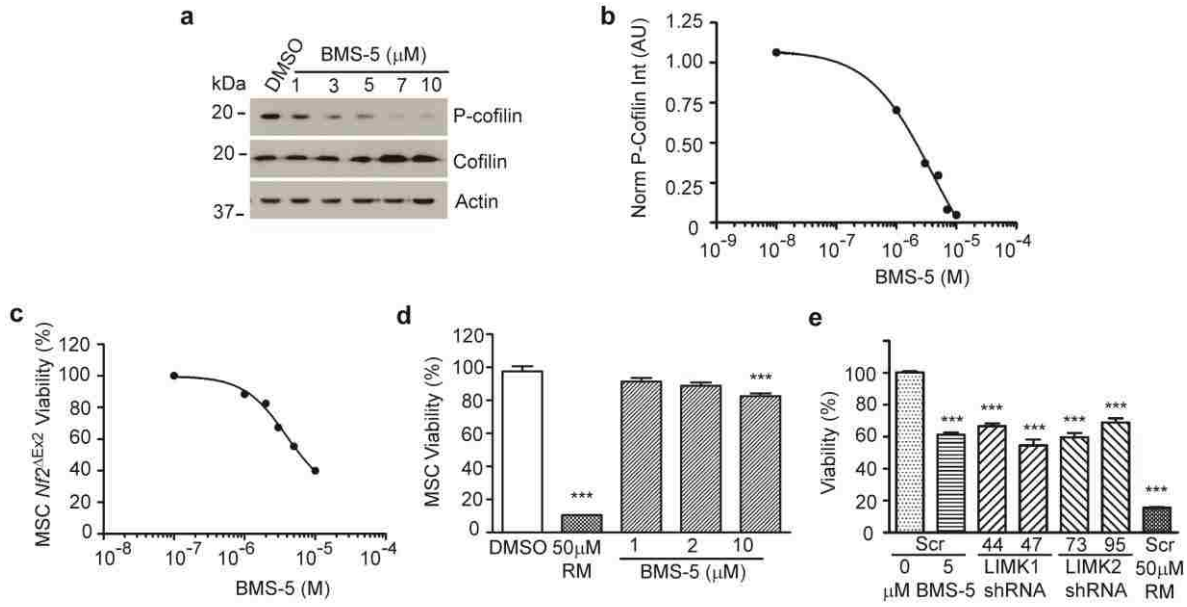

Figure 4. LIMK Inhibition by BMS-5 or Silencing by shRNA in *Nf2$^{\Delta Ex2}$* MSCs Decreases Cell Viability.

(a) BMS-5 dose-response western blot. *Nf2$^{\Delta Ex2}$* MSCs were plated in 12-well plates. Cultures were treated the next day as indicated for 30 min. Cells were harvested, lysed and analyzed by western blotting for phospho-Ser3-cofilin and total cofilin. β-actin levels were used as loading controls for normalization. Representative blot of three independent experiments. **(b)** BMS-5 dose-response curve of cofilin phosphorylation in *Nf2$^{\Delta Ex2}$* MSCs. Analyzed as log [inhibitor] vs. response, variable slope (four parameters). **(c)** BMS-5 dose viability-response curve. *Nf2$^{\Delta Ex2}$* MSCs were seeded at 5 000 cells/well in 20 μl growth medium phenol-red free in a 384-well plate and after attachment were incubated with BMS-5 for 24 hrs. Cell viability was measured with the CellTiter-Fluor assay. Graph represents the mean ± SEM of 3 independent experiments analyzed together (n=96) log [inhibitor] vs. response, variable slope (four parameters). **(d)** BMS-5 viability response of control MSCs. Cell viability was measured as in (c). Graph represents the mean ± SEM (n=16). DMSO control was considered 100% viability. Rapamycin (RM) (50 μM) was a positive control for cell death. ****P*<0.001 determined by one-way ANOVA using Dunnett's multiple comparison test. **(e)** Viability of *Nf2$^{\Delta Ex2}$* MSCs expressing LIMK 1 or LIMK2 shRNAs were compared to cells expressing scrambled shRNA untreated or treated with 5 μM BMS-5 or 50 μM rapamycin (RM) for 24 hrs in a 384-well format. Cell viability was measured with the CellTiter-Fluor assay. *Nf2$^{\Delta Ex2}$* MSCs expressing scrambled shRNA represented 100% viability, and the 50 μM RM treated cells were a positive control for cell death. Graph represents the mean ± SEM of 4 independent experiments analyzed together (n=128). ****P*<0.001determined by one-way ANOVA using Dunnett's multiple comparison test.

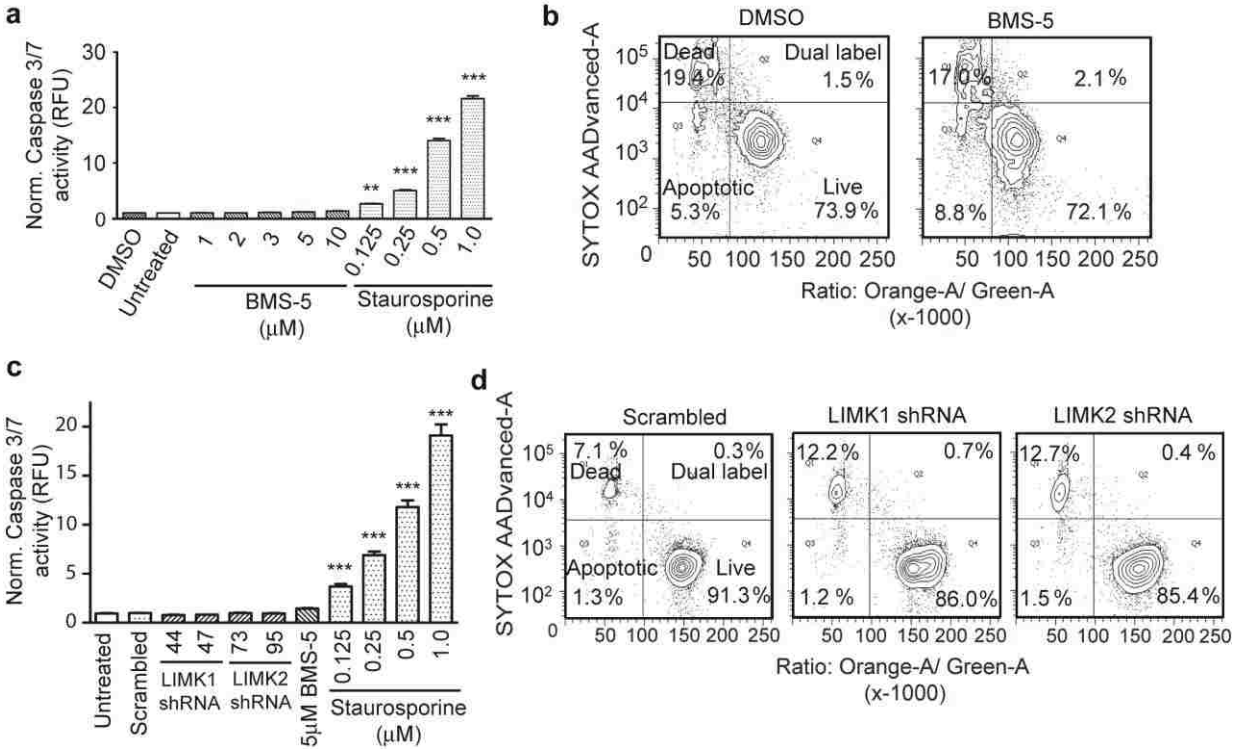

Figure 5. Inhibition or Silencing of LIMK does not Induce Apoptosis.

(a) Caspase 3/7 activity assay. *Nf2*$^{\Delta Ex2}$ MSCs were seeded at 5 000 cells/well in 20 μl growth media, phenol-red free in a 384-well plate and incubated for 16 hrs at 37ºC, 7% CO_2. Next, 5 μl/well of the indicated solution was added and incubated for 8 hrs. Caspase 3/7 activity was measured with the ApoONE Homogeneous assay. Staurosporine curve was used as positive control. Histogram represents 3 independent experiments (n=96) normalized to untreated and analyzed together. ***P*<0.01; ****P*<0.001determined by one-way ANOVA using Dunnett's multiple comparison test. **(b)** *Nf2*$^{\Delta Ex2}$ MSCs plated in a 6-well format were incubated with 2 μM BMS-5 or DMSO vehicle for 24 hrs. Plasma membrane asymmetry was evaluated with the Violet ratiometric assay by flow cytometry. Densitometry graph illustrates the following quadrants: apoptotic (Q3), dead (Q1), live (Q4) and dual label (Q2). **(c)** Caspase 3/7 activity measured with the ApoONE assay of *Nf2*$^{\Delta Ex2}$ MSCs uninfected or infected with control scrambled or the indicated constructs for LIMK1/2 shRNA silencing. Cells were incubated 24 hrs in a 384-well format and in the presence of inhibitors for 8 hrs where indicated. Staurosporine response was used as positive control. Histogram represents 5 independent experiments normalized to scrambled control and analyzed together (n=160). ****P*<0.001determined by one-way ANOVA using Dunnett's multiple comparison test. **(d)** *Nf2*$^{\Delta Ex2}$ MSCs infected with scrambled shRNA or shRNAs targeting LIMK1/2 constructs were plated in a 6-well format and incubated for 24 hrs. Plasma membrane asymmetry was assessed with the Violet ratiometric assay by flow cytometry in three independent experiments. Densitometry plots show the quantification of the population distribution into the four quadrants as in (b).

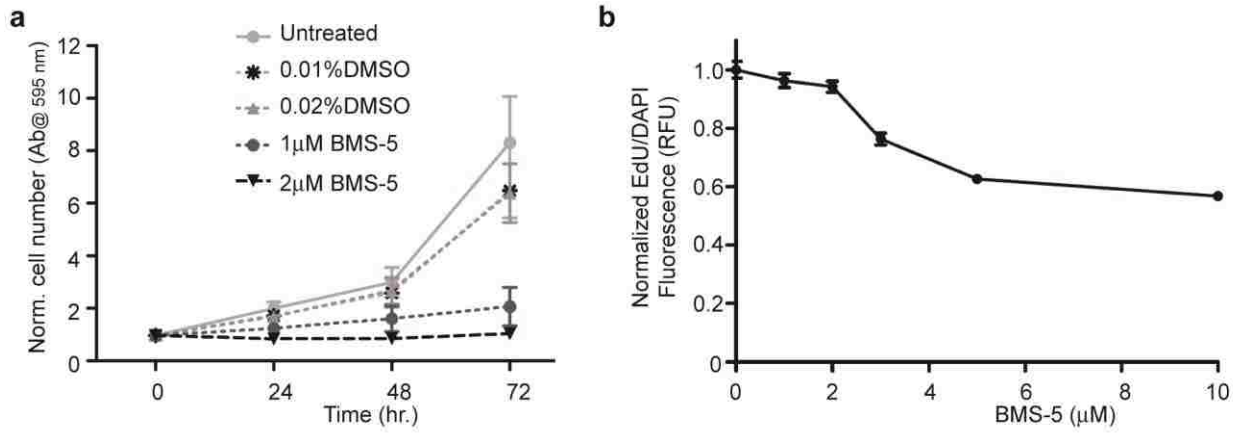

Figure 6. BMS-5 Decreases *Nf2*$^{\Delta Ex2}$ MSC Proliferation and DNA Synthesis in a Dose-Dependent Manner.

(a) *Nf2*$^{\Delta Ex2}$ MSCs were grown in 24-well plates. Cell proliferation was measured at 0; 24; 48 and 72 hrs time points after incubation with BMS-5 or DMSO vehicle. The number of cells at each time point was assessed with the crystal violet assay. Graph combines 3 independent experiments in triplicates (mean ± SEM, n=9). **(b)** *Nf2*$^{\Delta Ex2}$ MSCs were treated with the indicated BMS-5 concentrations for 24 hrs. EdU was added to the culture for the last 6 hours. Incorporation of EdU into S-phase cells was assessed with the EdU Click-It microplate assay and fluorescence was measured on a plate reader. Graph combines 3 independent experiments (mean ± SEM, n=44).

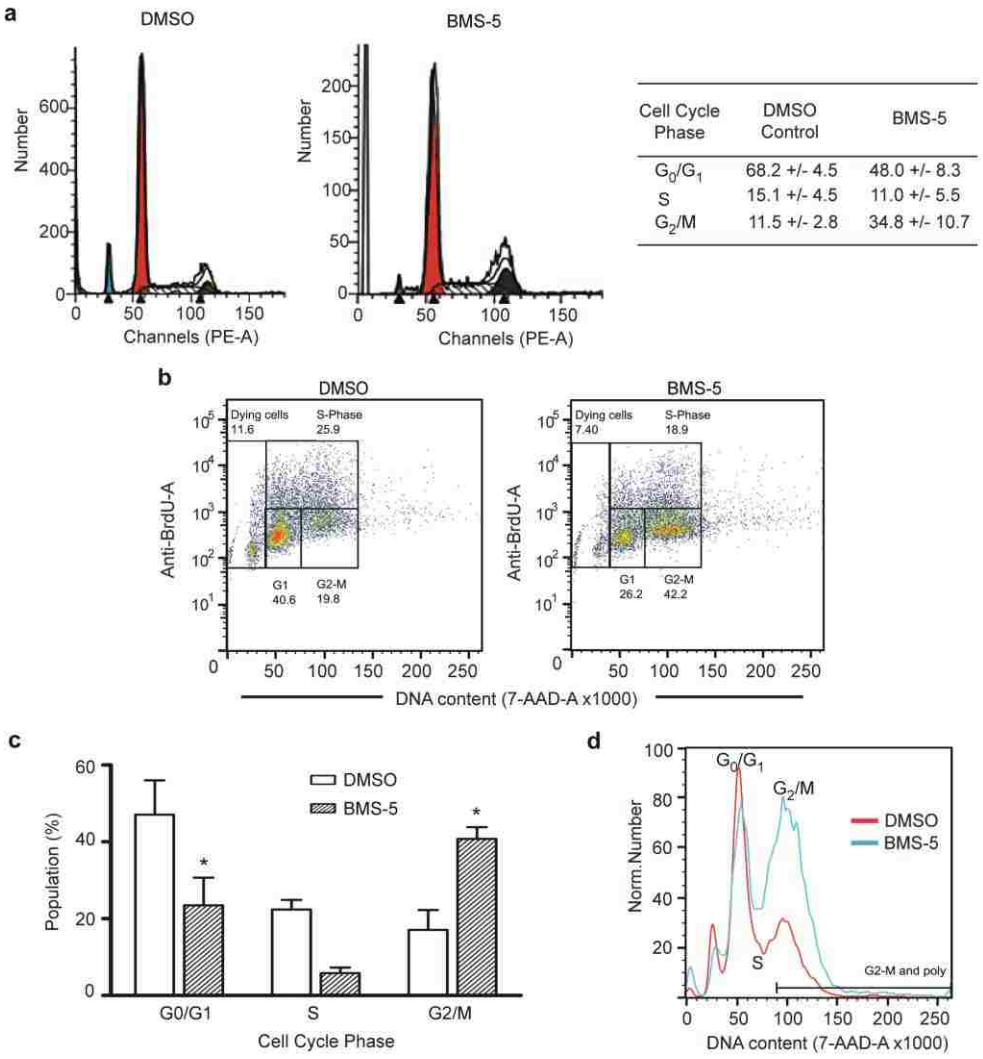

Figure 7. Inhibition of LIMK Interferes with Cell Cycle Progression of *Nf2*$^{\Delta Ex2}$ MSCs.

(a) *Nf2*$^{\Delta Ex2}$ MSCs were grown in a 6-well format and treated with 5 µM BMS-5 for 7 hours prior to labeling. Cells were analyzed by flow cytometry. Propidium iodide labeling profile of the diploid cell population analyzed with the ModFit program. Tabulation of the distribution of cell cycle phases of 3 independent experiments (mean± SEM, n=3). **(b)** *Nf2*$^{\Delta Ex2}$ MSCs were treated with 5 µM BMS-5 or DMSO control overnight prior to 3 hr BrdU labeling and analysis by flow cytometry. Distribution of BrdU- and 7-AAD-labelled cells analyzed with FlowJo software. These distribution plots are representative of 4 independent experiments (n=4). **(c)** Graph of the distribution of the cell cycle phases of all the experiments as mean ± SEM, **P*<0.05 determined by two-way ANOVA and Bonferroni multiple comparisons post-test. **(d)** Overlay of histograms of 7-AAD content comparing the vehicle and BMS-5 treated cells shown in (b).

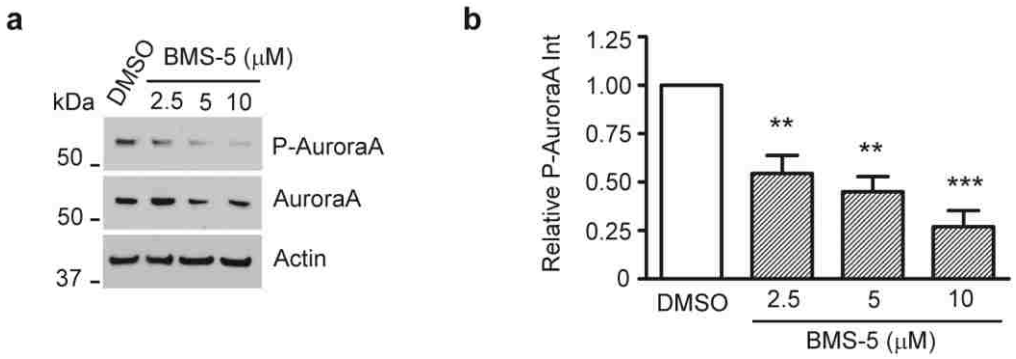

Figure 8. Inhibition of LIMKs Decreases Aurora A Autophosphorylation.

(a) Representative western blot of three independent BMS-5 dose-response experiments. *Nf2*$^{\Delta Ex2}$ MSCs were plated in half of a 12-well plate and treated the next day with increasing BMS-5 concentrations or DMSO for 8 hr. Cells were harvested, lysed and 10 μg of protein were analyzed by western blotting for phospho-Thr288-Aurora A and Aurora A. β-actin levels were used as loading controls. **(b)** Quantification of BMS-5 effect-response on Aurora A phosphorylation. Graph represents the mean ± SEM (n=3), ***P*<0.01; *** *P*<0.001 determined by one-way ANOVA using Dunnett's multiple comparison test.

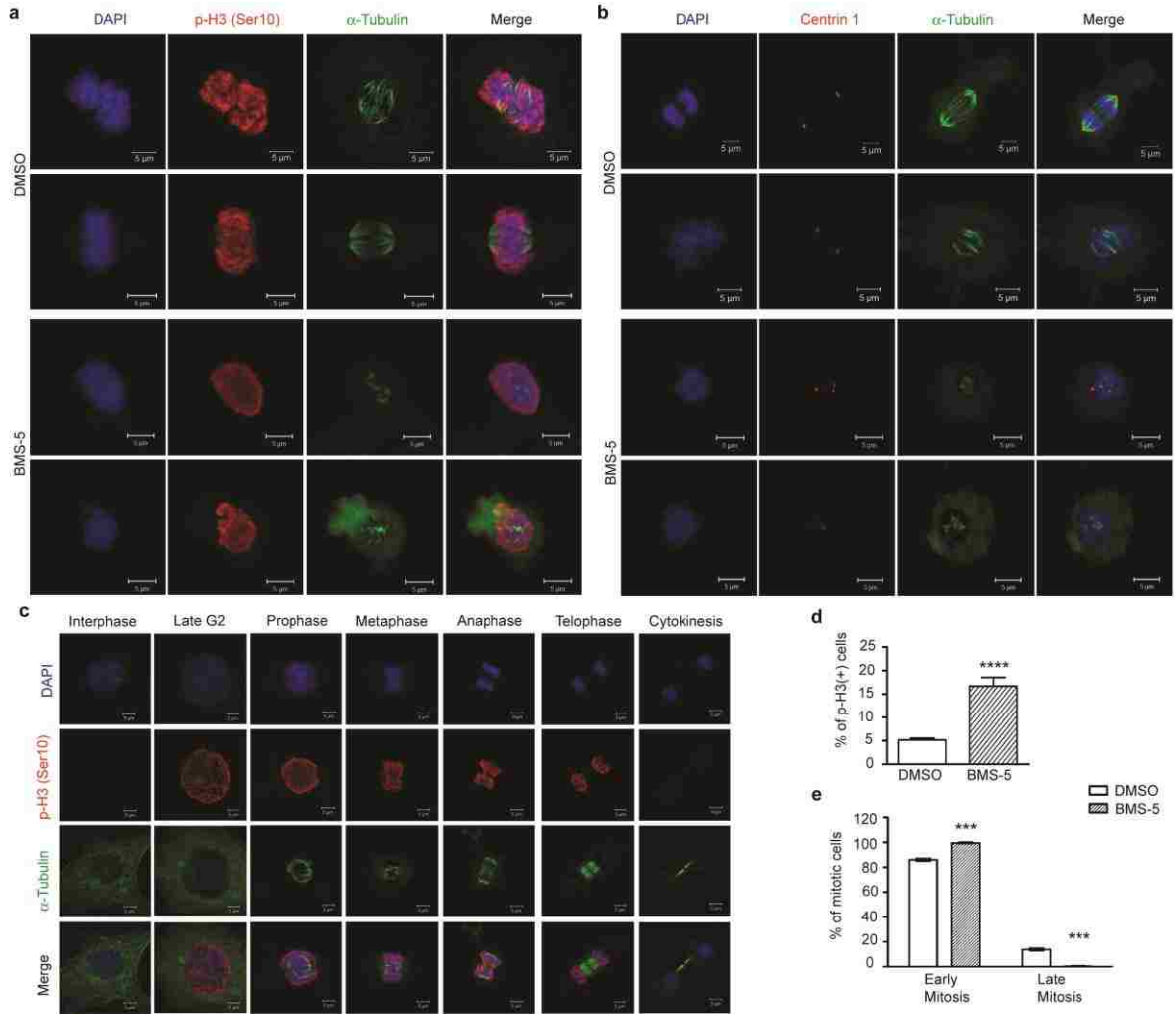

Figure 9. Inhibition of LIMKs Produce Abnormal Spindle and Centrosome Assemblies.

Representative confocal images of *Nf2*$^{\Delta Ex2}$ MSCs grown overnight on glass coverslips and treated with 4 μM BMS-5 or 0.04% DMSO for 8 hrs , fixed and immunostained with α-tubulin (green) and (a) P-H3(ser10) or (b) centrin1 (red). Nuclei were visualized with DAPI (blue). (c) Representative confocal images of DMSO treated *Nf2*$^{\Delta Ex2}$ MSCs depicting the cell cycle phases considered for analysis. (d) Quantification of the percentage of cells in late G_2/M phase assessed by positive p-H3 immunostaining. **** P<0.0001 determined by unpaired t test, two-tailed, from triplicate coverslips of three independent experiments (n=9). (e) Quantification of the percentage of mitotic cells in early (pro/metaphase) and late (ana/telophase) mitosis. *** P<0.001 determined by two-way ANOVA and Bonferroni multiple comparisons post-test. Scale bar: 5 μm.

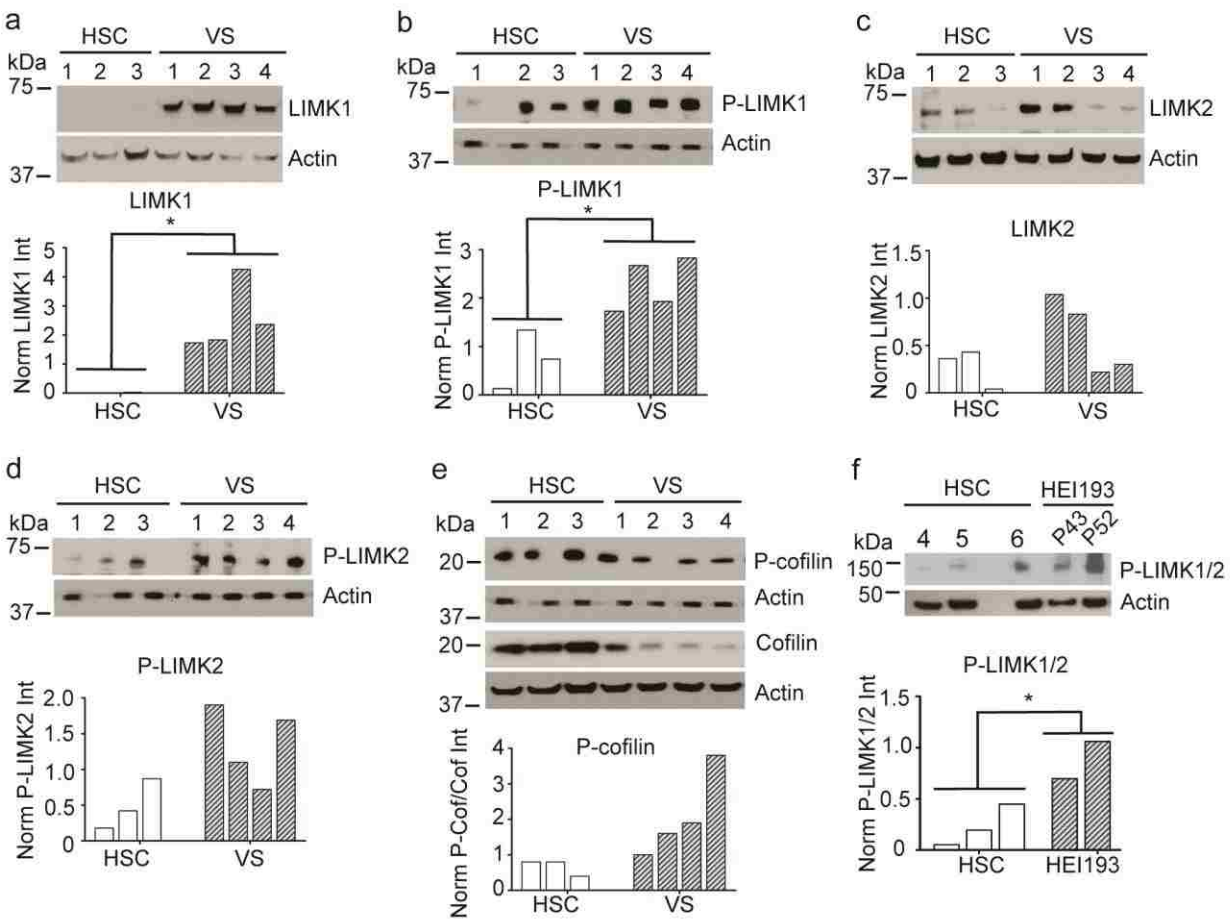

Figure 10. LIMKs are Overexpressed in Human Vestibular Schwannomas.

Lysed cultured human Schwann cells (HSC) cultured in 100-mm dishes and homogenized frozen human sporadic vestibular schwannomas (VS) were resolved by SDS-PAGE and analyzed by western blot. Quantitation of the western blots was done by densitometry analysis with ImageJ software, normalized to β-actin and is plotted below. Western blots for **(a)** LIMK1, **(b)** phospho-Thr508-LIMK1, **(c)** LIMK2, **(d)** phospho-Thr505-LIMK2 and **(e)** phospho-Ser3-cofilin and cofilin. β-actin was used as a loading control. *P<0.05 determined using unpaired t-test of HSC vs. VS populations, two-tailed. **(f)** HSCs from normal individuals (control) and HEI193 cells at P43 and P52 were cultured in 60-mm dishes and analyzed by western blotting for phospho-Thr508/505-LIMK1/2. β-actin was used as a loading control.

CHAPTER THREE: INHIBITION OF SIRT2 ACTIVITY SELECTIVELY REDUCES VIABILITY OF *Nf2*$^{\Delta Ex2}$ MOUSE SCHWANN CELLS

Introduction

Neurofibromatosis type 2 (NF2) is a benign tumor disorder of the nervous system caused by mutations in the NF2 gene that encodes a tumor suppressor called schwannomin or merlin. The hallmark of NF2 is the formation of bilateral schwannomas in the vestibular branch of the auditory nerve. Patients frequently develop additional schwannomas in other cranial, spinal and peripheral nerves as well as meningiomas and ependymomas. Common initial symptoms include hearing loss, dizziness or imbalance; however life-threatening compression of the brainstem also occurs [2]. The choices for NF2 schwannoma treatments are surgical resection or stereotactic radiosurgery. Many schwannomas however are inoperable and surgery often causes complete loss of nerve function, while radiosurgery carries an increased risk of a future secondary malignancy [1]. Currently, a few clinical trials of anti-cancer drugs are underway for NF2 [71, 91]. Molecular studies of merlin's mechanism of action have revealed that merlin regulates signaling from mitogenic, adhesion and extracellular matrix receptors through many essential signaling pathways [7, 72]. However, the pleiotropic effect of merlin has made it difficult to identify the most relevant drug targets.

As an alternative approach to drug discovery, we conducted an unbiased high-throughput screen of the library of Pharmacologically Active Compounds (LOPAC) using viability of *Nf2*$^{\Delta Ex2}$ mouse Schwann cells (MSC) as a phenotypic assay to identify

potential compounds and pathways relevant to NF2 schwannoma treatment. One compound identified in the screen was AGK2, a SIRT2 inhibitor. SIRT2 is one of seven mammalian sirtuins, also known as class III HDACs (histone deacetylases). Sirtuins are NAD(+) dependent deacetylases, that remove the acetyl group from the lysine's epsilon-amine in a multi-step reaction[44, 92]. SIRT2 is mainly cytoplasmic and its known substrates include: α-tubulin, partitioning defective 3 homolog (PAR3), p53, K-RAS, histone H4K16, forkhead Box O1 and 3a (FOXO1 and 3a) and RIP1 [45, 50, 52, 60, 61, 67]. While beneficial effects of SIRT2 inhibition was shown in neurodegenerative diseases such as Parkinson's and Huntington's disease, the role of SIRT2 in cancer remains controversial [51, 53]. SIRT2 has been reported to function as a tumor suppressor that is down-regulated in some human gliomas; however, its function has also been reported as essential for survival of C6 glioma cells. Small molecule SIRT2 inhibitors have in some cases selectively induced tumor cells death [58, 63-66].

Here we validate AGK2 as a compound that selectively reduces viability of *Nf2*$^{\Delta Ex2}$ MSC compared to normal MSCs. Moreover we demonstrate differential expression levels of SIRT2 in *Nf2*$^{\Delta Ex2}$ versus normal MSCs that are associated with a general reduction in lysine acetylation. Phenotypic mechanism of action studies suggests that inhibition of SIRT2 in *Nf2*$^{\Delta Ex2}$ SCs triggers a necrotic pathway.

Materials and Methods

Inhibitors

The SIRT2 inhibitors AGK-2; CAS name 2-Cyano-3-[5-(2,5-dichlorophenyl)-2-furanyl]-N-5-quinolinyl-2-propenamide and AK1; CAS name 3-(azepan-1-ylsulfonyl)-N-(3-nitrophenyl) benzamide were purchased from Sigma-Aldrich and Cayman Chemicals. Rapamycin and Staurosporine were from Santa Cruz Biotechnology (Santa Cruz, CA).

Antibodies

β-Actin (8H10D10) and α-tubulin (DM1A) mouse mAb, Merlin (D1D8), acetylated-lysine (A-K^2-100), Acetyl-α-tubulin (Lys40) (D20G3)XP, SIRT1(D1D7), SIRT3(D22A3), SIRT5(D8C3), SIRT7(D3K5A) and LC3B(D11)XP rabbit mAb, HMGB1 rabbit Ab were purchased from Cell Signaling (Danvers, MA). GAPDH mAb was from Millipore. SIRT2 rabbit Ab was from Sigma-Aldrich. S-100 rabbit Ab was purchased from Dako Cytomation (Glostrup, Denmark). Secondary antibodies, peroxidase-conjugated goat anti-mouse IgG and goat anti-rabbit-IgG, were purchased from Pierce, Thermo Fisher (Rockford, IL). Goat anti-rabbit-IgG Alexa -Fluor488 and -Fluor546 conjugated antibodies were purchased from Invitrogen (Grand Island, NY).

Mouse Schwann Cell Culture

MSC were cultured on 200 µg/ml poly-L-lysine hydrobromide (PLL, Sigma-Aldrich), and 10 µg/ml Laminin (Invitrogen) coated 60 or 100-mm Corning dishes. MSC

growth medium: DMEM:F12 1:1 (Gibco) plus 1X-N2 supplement (Gibco), 2µM forskolin, 10 ng/ml neuregulin and 1% Penicillin/Streptomycin (Gibco).

$Nf2^{\Delta Ex2}$ Mouse Schwann Cell Culture

$Nf2^{\Delta Ex2}$ MSC generated in the lab were cultured in CellBIND-Corning 100 mm dishes. *$Nf2^{\Delta Ex2}$* MSC growth medium was DMEM/F12 1:1 (Gibco); 1X-N2 supplement (Invitrogen) and 1% Penicillin/Streptomycin. All protocols are in accordance with guidelines of and approved by the University of Central Florida (UCF) Institutional Animal Care and Use Committee (IACUC). UCF vivarium is International-certified by the Association for Assessment and Accreditation of Laboratory Animal Care.

Human Schwann Cell and HEI193 Cell Cultures

Vials of frozen human SCs were thawed and seeded on coated 60 mm Corning plates (200 µg/ml PLL and 50 µg/ml Laminin) containing D10M growth medium: DMEM (Gibco) plus 10% heat inactivated fetal bovine serum (HIFBS, HyClone, Logan, UT), 2 µM Forskolin (Sigma), 0.02 mg/ml Pituitary Extract (Biomedical Tech. Inc) and 1% Penicillin/Streptomycin (Gibco). HEI193 cells were purchased from ATCC (Manassas, VA). HEI193 growth medium: DMEM plus 10% HIFBS, 1% Penicillin/Streptomycin.

Western Blot Analysis

SCs were lysed in modified RIPA buffer (25 mM Tris-HCl pH 7.6; 150 mM NaCl: 1% Triton X-100, 1% Sodium dodecyl sulfate (SDS) with protease inhibitor cocktail and phosphatase inhibitor cocktails 2 and 3, Sigma-Aldrich). To remove cell debris, lysates

were centrifuged at 15,000 rpm for 10 min at 4°C. Protein concentration of the supernatant was determined with the DC Assay (BioRad, Hercules, CA). 10–15 µg of sample protein was resolved in 4–20% polyacrylamide gels (Pierce), transferred to a polyvinylidene fluoride **(**PVDF) membrane (Immobilon-P, Millipore, Bedford, MA), blocked with 5% BSA and incubated overnight at 4°C with anti- acetylated-lysine (1:500), Acetyl-α-tubulin (Lys40) (1:1,000), α-tubulin (1:1,500), SIRT1(1:500), SIRT2 (1:500), SIRT3(1:500), SIRT5(1:500), SIRT7(1:500), HMGB1 (1:500) for cell lysates and at (1:250) for concentrated medium, GAPDH (1:10,000), LC3B (1:500) and β-Actin (1:15,000) primary antibodies, followed by their corresponding secondary antibodies at 1:20,000. Quantification of western blots was done by densitometry using NIH ImageJ software.

Immunofluorescence

Control and *Nf2*$^{\Delta Ex2}$ MSC were plated on coated German glass coverslips (200 µg/ml PLL and 10 µg/ml Laminin) and immunostained as previously described [81](Thaxton, Bott et al. 2011). Images were acquired using a Zeiss LSM710 Confocal microscope with 3 spectral detection channels, 5 laser lines - 458, 488, 514,543 & 633 nm, FL filter set 49 DAPI, EX G365, FL filter set 43 CY 3, FL filter set 38 Endow GFP, all shift free, EC Plan-Neofluar 40x/1.3 DIC WD=0.21 M27 objective lens, with the ZEN2009 software. Fluorescence signals were acquired on separate channels with identical parameters for each labeled protein from a single plane. Fluorescence intensity

of the green channel was done using Volocity software. Pictures were processed with the ZEN2011 software in the same manner.

Cell Viability Assay

Viability of dose-response assays was assessed with the CellTiter-Fluor cell viability assay (Promega) following manufacturer's specifications. Normal MSC and *Nf2*$^{\Delta Ex2}$ MSC were seeded at 5,000 cells/well in 20 µl of phenol-red free growth medium in 384-well plates (black with clear bottom, CellBIND-Corning) and centrifuged 1 min at 500 rpm. Cultures were incubated at 37ºC, 7% CO2 until attachment (2.5–3.5 hours), then 5 µl of compound/vehicle solution was added to each well. Plates were quick spun again and returned to the incubator for 24 hours. Fluorescence was read with a Synergy H1 Hybrid plate reader (BioTek, Winooski, VT).

Proliferation Assays

For the 72 hours cell proliferation study, cell numbers were assessed with the Crystal Violet Assay as previously described [82]. Equal number of *Nf2*$^{\Delta Ex2}$ MSC were seeded in 24-well plates and cell number was evaluated at 0; 24; 48 and 72 hour time points. Absorbance at 595 nm was measured with a µQuant plate reader (BioTek).

Rate of DNA synthesis was evaluated at 24 hours with the Click-iT EdU Microplate Assay (Invitrogen/ Life Technologies) as previously described [93]. Oregon green-488 and DAPI fluorescence was measured with a Synergy H1 hybrid plate reader.

Cell Cycle Analysis

The cell cycle was analyzed by flow cytometry with propidium iodine (PI) staining and BrdU/7AAD. PI staining was performed on ethanol fixed cells using PI/RNase solution from Beckton-Dickinson and studied on a BD Canto-II flow cytometer. Histograms were analyzed with ModFit LT software (Verity Software House, Topsham, ME). For each sample, 10,000 events were collected and the diploid population was distributed across G_0/G_1, S and G_2/M phases.

The BrdU/7AAD assay kit was purchased from Beckton-Dickinson. Cells were seeded in 6-well plates and treated overnight with inhibitor/vehicle. On the next day, 10 µM BrdU was added to the cultures for 3 hours, cells were harvested, fixed and analyzed following manufacturer's instruction. The BD Canto-II flow cytometer with the BD FACSDiva™ 6.1.3 software was use for acquisition and Kaluza 1.2 (Beckman Coulter) software for data analysis.

Apoptosis Assays

For caspases dependent apoptosis the caspase activity was assessed by the Apo-ONE homogeneous Caspase-3/7 assay (Promega) following manufacturer's specifications. For caspases dependent and/or independent apoptosis the membrane asymmetry was measured with the Violet Ratiometric Membrane Asymmetry Probe/Dead Cell Apoptosis Kit (Invitrogen/Life Technologies). Both assay were previously described [93].

Cytotoxicity Assays

Cytotoxicity was assayed in a 384 well plate format with 5,000 cells/well after 24 hours incubation with the inhibitors/vehicle with the CellTox Green assay (Promega), following the express, no-step addition at seeding method described by the manufacturer. Cells treated with 27 µg/ml digitonin were considered 100% cytotoxicity control. Fluorescence (Ex= 510nm/Em= 532 nm) was measured on a Synergy H1 Hybrid plate reader.

LDH Release Assay

LDH released into the culture medium was measured with the CytoTox-ONE assay (Promega). *Nf2*$^{\Delta Ex2}$ MSC were seeded at 4,000 cell/well in 384 well plates and were treated on the next day with increasing doses of inhibitor/vehicle and incubated for 4 hours. Positive 100% cytotoxicity control was 27 µg/ml digitonin. Plate and assay reagent were equilibrated to room temperature for 25 min and after addition of 25 µl of assay reagent, the plate is incubated at room temperature in the Synergy H1 Hybrid plate reader. No stop solution was used. Fluorescence (Ex=560 nm/Em= 590nm) was measured 5 min after the first column received reagent.

HMGB1 Release Assessment

Equal number of *Nf2*$^{\Delta Ex2}$ MSC per well in CellBIND 6-well plates were cultured overnight. On the next day the medium was replaced with 2 ml treatment medium containing SIRT2 inhibitors/vehicle in duplicate wells and incubated for 6 hours at 37ºC,

7% CO2. Then working on ice, media from duplicates were pooled and transferred to cold 15 ml conical tubes, centrifuged for 5 min at 800g, 4 ºC. The supernatant (~4ml) was syringe filtered with 0.45 µm filter (Fisher), transferred to cold 7 ml 9K MWCO Pierce concentrators (Thermo Scientific) and centrifuged for 30 min at 4,000g, 4 ºC. From 120 to 150 µl of concentrated proteins were obtained and prepared for SDS-PAGE. When media was removed from cultures, the plates were washed once with ice cold PBS and cell were lysed with the modified RIPA buffer mentioned above; protein concentration was measured with the DC assay (BioRad). Equal volume of concentrated proteins from medium and 10 µg of protein of cell lysates were analyzed by western blotting for HMGB1.

Statistical Analysis

GraphPad Prism version 5.0 for Windows (GraphPad, La Jolla, CA, USA) was used for statistical analysis and graph generation. AGK-2 and AK1 dose-response experiments were analyzed by non-linear regression (four parameters). Experimental data from three independent experiments were statistically analyzed by one or two-way ANOVA with post-tests, as indicated for each experiment.

Results

Nf2$^{\Delta Ex2}$ MSC have Higher SIRT2 Levels and Lower Lysine Acetylation Levels than Control MSC.

Nf2$^{\Delta Ex2}$ mouse Schwann cells (MSC) contain a deletion of exon 2 of the *Nf2* gene that replicates a documented patient mutation. *Nf2$^{\Delta Ex2}$* MSC were created by in vitro adeno-Cre transduction of mouse Schwann cells isolated from sciatic nerves of homozygous *Nf2$^{flox2/flox2}$* mice as previously described [81, 83, 93]. Using this NF2 cell model, we screened the Library of Pharmacologically Active Compounds (LOPAC, Sigma-Aldrich) searching for compounds capable of reducing their viability. One of the initial hits we chose to investigate was AGK2, a small molecule SIRT2 inhibitor. The sirtuin family of deacetylases has not been examined heretofore in NF2.

To visualize the lysine acetylation patterns in *Nf2$^{\Delta Ex2}$* MSC and control MSC, we performed a western blot using an ε-acetyl-Lysine antibody. Control MSC had a higher number of and more intensely acetylated bands than *Nf2$^{\Delta Ex2}$* MSC (Figure 11 a, and Supplementary Figure 3). Because the *Nf2$^{\Delta Ex2}$* MSC presented fewer bands, we asked whether SIRT2, the target of AGK2 had altered expression levels. Indeed we found that *Nf2$^{\Delta Ex2}$* MSC expressed SIRT2 at higher levels than control MSC (Figure 11 b). The acetyl-lysine blot differed greatly around the 50 kDa molecular weight marker. Because SIRT2 is a recognized acetyl-α-tubulin deacetylase, we investigated if any of those bands were α-tubulin. *Nf2$^{\Delta Ex2}$* MSC have highly deacetylated tubulin levels compared to control MSC (Figure 11 b). We confirmed these differences with several independently derived *Nf2$^{\Delta Ex2}$* MSC lines (Figure 11 c). We next immunoblotted for glyceraldehyde-3-

phosphate dehydrogenase (GAPDH) because tumor cells have altered metabolism and sirtuins can influence metabolic and energetic regulation. We found higher levels of GAPDH in *Nf2*$^{\Delta Ex2}$ MSC compared to MSC consistent with higher glycolytic activity in *Nf2*$^{\Delta Ex2}$ MSC than controls (Figure 11 c). In order to validate the results in our cellular model, we measured SIRT2 and acetyl-α-tubulin levels in a human NF2 cell line created by immortalization of schwannoma cells from a NF2 patient with the E6 and E7 genes of the papillomavirus [85]. Similarly, we found higher levels of SIRT2 in HEI-193 cells than in control human Schwann cells which correlated with lower acetylated tubulin levels in HEI-193 compared to control cells (Figure 11 d).

We localized SIRT2 in control and mutant cells using immunofluorescence staining followed by confocal microscopy. Both cells types expressed the Schwann cell marker S100 and control MSC immunoreacted with the N-terminal merlin antibody whereas the *Nf2*$^{\Delta Ex2}$ MSC did not. Both cell types expressed SIRT2 in the cytosol and nuclei, however, *Nf2*$^{\Delta Ex2}$ MSC in general had higher levels of fluorescence intensity than controls. Control MSC showed significantly higher levels of acetylated tubulin compared to *Nf2*$^{\Delta Ex2}$ MSC and in the latter, the weak immunofluorescence signal for acetylated tubulin was mostly perinuclear (Figure 11 e).

Lastly, we examined the expression of other sirtuin family members by western blotting. SIRT5 was expressed in control and *Nf2*$^{\Delta Ex2}$ MSC at similar levels, whereas SIRT1, SIRT3 and SIRT7 were expressed at higher levels in *Nf2*$^{\Delta Ex2}$ MSC than MSC (Figure 11 f).

SIRT2 Inhibition Selectively Reduces Nf2$^{\Delta Ex2}$ MSC Viability in a Dose-Dependent Manner

To evaluate selectivity of SIRT2 inhibition for *Nf2*$^{\Delta Ex2}$ MSC viability, we conducted a dose response study of AGK2 using CellTiter-Fluor assay. We found that a 24 hour exposure to AGK2 decreased *Nf2*$^{\Delta Ex2}$ MSC viability in a dose-dependent manner with an IC_{50}= 9.0 μM (Figure 12 a). In contrast, AGK2 did not decrease control MSC viability as effectively as for *Nf2*$^{\Delta Ex2}$ cells (Figure 12 b). At 10 μM AGK2, *Nf2*$^{\Delta Ex2}$ cells retained 45.8 ± 0.7 % viability compared to control MSC that retained 70.9 ± 1.8 % viability.

Although AGK2 is a highly selective SIRT2 inhibitor, it does minimally inhibit SIRT1 and SIRT3 at ten times the SIRT2 IC_{50} level when tested in vitro [51]. To corroborate that SIRT2 was specifically inhibited by AGK2 and associated with loss of *Nf2*$^{\Delta Ex2}$ MSC viability, we tested the effect of an alternative SIRT2 inhibitor, AK1. This benzylsulfonamide also inhibits SIRT2 enzymatic activity by targeting the nicotinamide binding site but with less potency for SIRT1 and SIRT3 than AGK2. We found that AK1 decreased *Nf2*$^{\Delta Ex2}$ MSC viability in a dose-dependent manner with an IC_{50}= 26.1 μM (Figure 12 c). AK1 minimally reduced control MSC viability which retained 82.8 ± 2.1% viability at 25 μM (Figure 12 d). These results suggest that pharmacological inhibition of SIRT2 selectively reduced *Nf2*$^{\Delta Ex2}$ MSC viability.

SIRT2 Inhibition Reduces Nf2$^{\Delta Ex2}$ MSC Proliferation without Interfering with Cell Cycle Progression or DNA Synthesis

We next assessed the ability of AGK2 to decrease cell viability for longer incubation times. We treated *Nf2*$^{\Delta Ex2}$ MSC with vehicle or inhibitor and assessed the cell

number by crystal violet staining at 24, 48 and 72 hours. We found that at 72 hours AGK2 significantly reduced the number of *Nf2*$^{\Delta Ex2}$ MSC compared to vehicle control (Figure 13 a). We also measured EdU incorporation in AGK2-treated *Nf2*$^{\Delta Ex2}$ MSC and found that it did not decrease DNA synthesis compared to vehicle treated controls (Figure 13 b).

To determine if the decrease in cell number caused by AGK2 was associated with inhibition of cell cycle progression, we performed flow cytometry analysis of propidium iodine (PI) labeled cells. We found that AGK2 did not significantly alter the distribution of diploid cells in the cell cycle, although there was a tendency to slightly increase the percentage of cells in the G_2/M phase (Figure 13 e). To further analyze the effect of AGK2 on cell cycle progression, we performed a BrdU/7-AAD assay. There was no significant change in the distribution of treated and untreated cell populations during the cell cycle after 24 hours (Figure 13 f). These results suggest that SIRT2 inhibition decreased *Nf2*$^{\Delta Ex2}$ MSC proliferation by mechanisms independent of interfering with cell cycle progression.

SIRT2 Inhibition Induces Nf2$^{\Delta Ex2}$ *MSC Cell Death*

To determine if SIRT2 inhibition reduced *Nf2*$^{\Delta Ex2}$ MSC viability by inducing apoptosis, we tested caspase 3/7 activity following AGK2 treatment. We found that AGK2 moderately increased caspase 3/7 activity at 10 μM compared to the positive control, staurosporine, that increased caspase 3 and 7 activity to much higher levels in a dose-dependent manner (Figure 14 a). To further analyze if SIRT2 inhibition induced

caspase independent apoptosis, we studied the effect of AGK2 on *Nf2*$^{\Delta Ex2}$ MSC membrane asymmetry using the violet ratiometric flow cytometry assay. We found AGK2 only moderately increased apoptosis from 3.5 ± 1.2 % in *Nf2*$^{\Delta Ex2}$ MSC treated with DMSO to 6.1 ± 2.8 % when treated with AGK2. This increase however was not statistically significant (Figure 14 b,c). These results suggest that even though AGK2 slightly induced apoptosis it is not the main mechanism responsible for the decreased viability of *Nf2*$^{\Delta Ex2}$ MSC.

Next, we assessed whether SIRT2 inhibition decreased *Nf2*$^{\Delta Ex2}$ MSC viability by inducing cell death by inducing cell necrosis. We measured cytotoxicity with a fluorescence plate format assay that uses a cyanine dye impermeant to live cells that stains DNA from dead cells and increases its fluorescence. We found that both, AGK2 and AK1, significantly increased the number of dead *Nf2*$^{\Delta Ex2}$ MSC in dose-dependent manners (Figure 15 a, b). To further analyze the mechanism of cell death, we measured the release of lactate dehydrogenase (LDH) from cells with damaged membranes into the medium with the CytoTox-ONE homogeneous membrane integrity assay. We found that both SIRT2 inhibitors, AGK2 and AK1 increased the levels of LDH released to the medium in a dose dependent manner. This is typically associated with cell necrosis (Figure 15 c,d). We also measured release from cells of the necrosis marker high mobility group box 1 protein (HMGB1) by western blot [94]. We found that AGK2 and AK1 induced release of significant amounts of HMGB1 into the medium that corresponded with a decrease in intracellular HMGB1 levels (Figure 15 e). To further characterize *Nf2*$^{\Delta Ex2}$ MSC cell death, we assessed the induction of autophagy by

immunoblotting for lipidated microtubule-associated protein 1 Light Chain 3 B (LC3B-II). Cytosolic LC3B-I during autophagy is lipidated by Atg 7 and 3 and is converted in LC3B-II that associates with autophagic vesicles [95]. We found that although DMSO slightly activates autophagy, neither AGK2 nor AK1 induced it (Figure 15 f).

These results suggest that SIRT2 inhibition decreased *Nf2*$^{\Delta Ex2}$ MSC viability by triggering cell death characterized by release of LDH and HMGB1.

Discussion

SIRT2 and Schwann Cells

SIRT2 was identified as a potential NF2 drug target from a pilot LOPAC screen. We confirmed that SIRT2 protein levels were higher in cultured *Nf2*$^{\Delta Ex2}$ MSC compared to cultured control MSC and that SIRT2 activity was essential for survival of *Nf2*$^{\Delta Ex2}$ Schwann cells but not wild type MSC. SIRT2 inhibition by AGK2 and AK1 selectively decreased viability of Schwann cells lacking functional merlin. The AGK2 and AK1 dose-dependent loss of cell viability correlated with a dose-dependent cell death that was further characterized as associated with release of the necrotic markers LDH and HMGB1 without induction of autophagy, cell cycle arrest or significant caspase 3/7 dependent or independent apoptosis.

Although SIRT2 has been considered a potential regulator of cell cycle progression [54-56, 96], we did not find evidence for that mechanism of action in this study. SIRT2 was reported to associate with mitotic structures and to increase in abundance and phosphorylation during mitosis. It has been reported to prevent

chromosome condensation and entry into M phase in response to mitotic stress. Additionally, overexpression of catalytically inactive SIRT2 increased the number of multinucleated HeLa cells. However in the absence of stressors, SIRT2 activity was not required for cell cycle progression in HeLa and HEK293 cells [57]. In Schwann cells, selective inactivation of *Sirt2* during early embryogenesis did not reduce the number of Schwann cells produced during the period of rapid cell proliferation that occurs at post-natal days 1-5. This supports the conclusion that cell cycle progression in Schwann cells is independent of SIRT2 activity [50] in agreement with our finding that SIRT2 inhibition did not decrease $Nf2^{\Delta Ex2}$ MSC viability by arresting cell cycle progression but rather by inducing cell necrosis. There is evidence for a role of SIRT2 in necrosis. Nie et al. reported that AGK2 treatment of PC12 cells decreased intracellular ATP levels and increased necrosis without affecting autophagy [97]. Additionally, tumor necrosis factor alpha (TNF-α) was shown to activate necroptosis via deacetylation of receptor-interacting protein 1 (RIP1) by receptor-interacting protein 3 (RIP3) bound SIRT2 allowing the formation of a stable complex in L929 and Jurkat T cells [67]. Due to the prominent role of cytokines in SC development and repair others have shown that while a low concentration of TNF-α induced SC proliferation, a high concentration of TNF-α induced SC growth arrest and apoptosis [98-100]. We have not studied TNF-α in $Nf2^{\Delta Ex2}$ Schwann cells and additional studies are needed to identify the pathway by which inhibition of SIRT2 activity leads to cell necrosis.

SIRT2 in Cancer

Similar to our findings in Schwannoma and control Schwann cells, upregulation of SIRT2 mRNA and protein levels has been reported in some cancer cells such as primary acute myeloid leukemia blasts compared to control hematopoietic progenitor cells from healthy individuals [101]. In glioma cells, however, it has been reported that several human glioma samples had reduced SIRT2 mRNA compared to normal brain tissue and that overexpression of SIRT2 decreased HTB14 glioma cells colony formation [64]. Notably, inhibition of SIRT2 activity decreased C6 glioma cells viability [63]. Additionally, aged mice with inactivation of the Sirt2 gene by deletion of exons 5-8 developed different types of tumors depending on their gender [58]. Treatment of C6 glioma cells with 10 μM AGK2 for 24 hours caused a 60% loss of viability due to both apoptosis and necrosis [63]. Similarly, another SIRT2 inhibitor, compound AC-93253 showed selectively decreasing viability of several human cancer cell lines over their human primary cells controls [65]. The panel included cell lines from prostate, pancreas, cervical and lung cancer. AC-93253 was also selectively cytotoxic to HeLa cells by inducing apoptosis and necrosis. Discrepancies in the positive and negative associations of SIRT2 with tumor development are likely due to differences in cell type, developmental activation patterns for SIRT2 and substrate preferences [50, 102]. For instance histone H4 is a principal substrate for SIRT2 in various cell types but not in oligodendrocytes [60, 103].

Inhibition of SIRT2 and other Deacetylases

Although AGK2 and AK1 selectively inhibit SIRT2, at higher concentrations they can also inhibit SIRT1 and SIRT3 in vitro [51]. Therefore it is possible that at the IC_{50} concentrations used in this study, the compounds could have also slightly decreased SIRT1 and 3 activity. Interestingly, treatment of BCL6-expressing Burkitt lymphoma cells and Burkitt lymphoma xenograft mice with a dual SIRT1 and SIRT2 inhibitor, cambinol, produced a potent antitumor effect [59]. Hence, there may be value to SIRT2 and SIRT1 combinatorial inhibition in schwannoma treatment. A recent study showed that acetylation of K-RAS at lysine104 attenuates its transforming activity in cancer cells and both SIRT2 and HDAC6 deacetylate K-RAS [61]. Moreover, α-tubulin and cortactin acetylation are regulated by SIRT2 and HDAC6 [45, 46, 104]. Due to the increasing interest of HDAC inhibitors in cancer, a new pan-HDAC inhibitor AR42 was tested on merlin null schwannoma and meningioma cells. Both *in vitro* and *in vivo* treatment showed a selective anti-proliferative effect on schwannoma and meningioma cells warranting further clinical evaluation for NF2 related tumors [105-107]. AR42, similar to other HDAC inhibitors also decreased Akt phosphorylation, a pathway upregulated in many cancers and NF2. Chen et al. have shown that AR42 targets HDAC1 and HDAC6 by disrupting their HDAC-protein phosphatase 1 (PP1) complexes, which leads to increased PP1-Akt association, and facilitates PP1-mediated dephosphorylation of Akt [108]. Therefore combinatorial inhibition of SIRT2 and HDAC6 could be evaluated when considering modulation of acetylation signaling for NF2 treatment.

We speculate that SIRT2 pharmacological inhibition may have some therapeutic value for NF2-associated schwannomas by promoting necrosis. However, additional research is needed to understand the relationship between merlin and SIRT2 in normal Schwann cells and the effect of merlin inactivation on protein acetylation and cell survival.

Figures

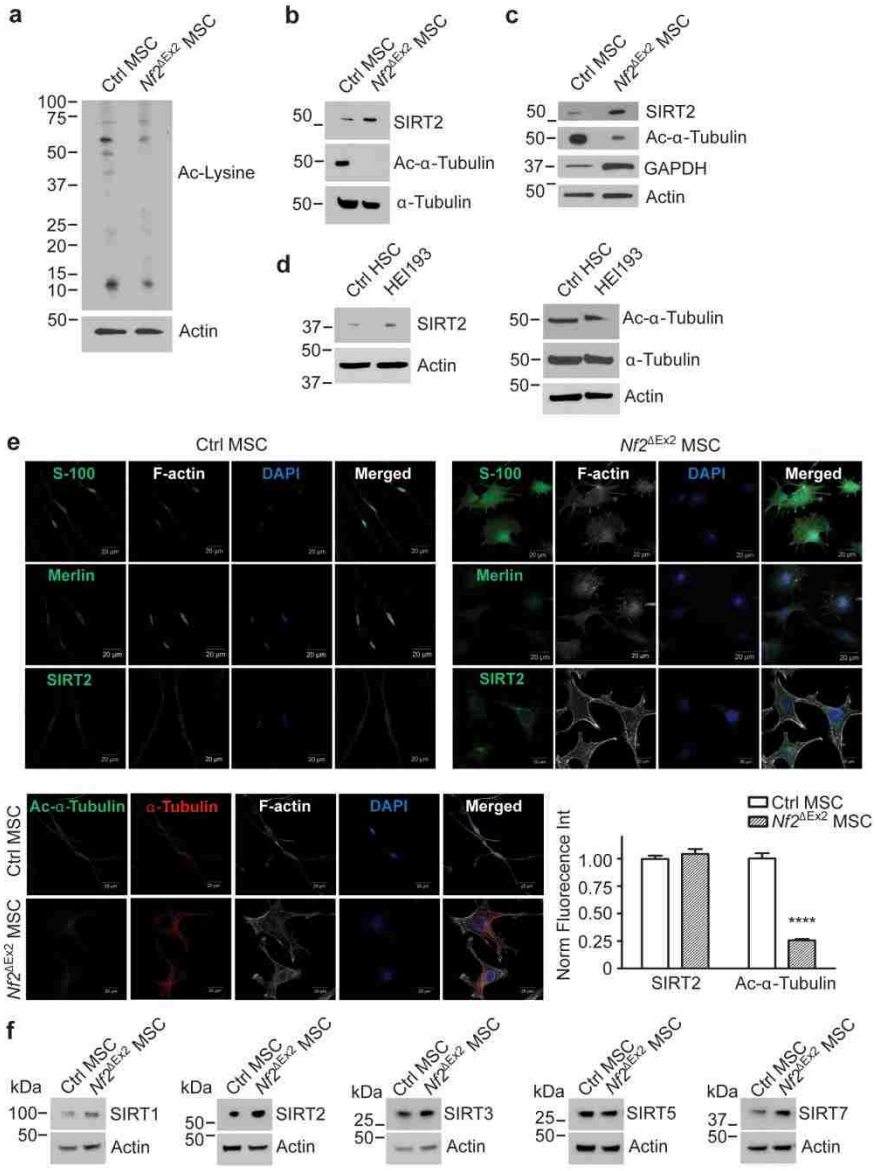

Figure 11. *Nf2*$^{\Delta Ex2}$ MSC Have Lower Levels of Lysine Acetylation and Higher Levels of SIRT2 Compared to Control MSC.

Control *Nf2*$^{flox2/flox2}$ MSC and *Nf2*$^{\Delta Ex2}$ MSC were analyzed by western blotting for: **a)** Acetyl-lysine, **b)** SIRT2, acetyl-α-tubulin, α-tubulin and **c)** SIRT2, GAPDH. Anti-β-actin was used as a loading control. **d)** Cultured control human Schwann cells (HSCs) from normal individuals and HEI193 cells were analyzed by western blotting for SIRT2, acetyl-α-tubulin, α-tubulin. Anti-β-

actin was used as a loading control. **e)** Representative confocal images of control MSC and *Nf2*$^{\Delta Ex2}$ MSC grown overnight on glass coverslips and immunostained with the indicated antibodies (green). The nucleus was visualized with DAPI stain (blue) and F-actin with phalloidin-Alexa633 (white). Scale bar: 20 µm. Quantitation of the immunofluorescence from three independent experiments was performed with Volocity software. ****P<0.0001 determined by two-way ANOVA using Bonferroni post-tests. **f)** Control *Nf2*$^{flox2/flox2}$ MSC and *Nf2*$^{\Delta Ex2}$ MSC were analyzed by western blotting for SIRT1, SIRT2, SIRT3, SIRT5, SIRT7 and β-actin.

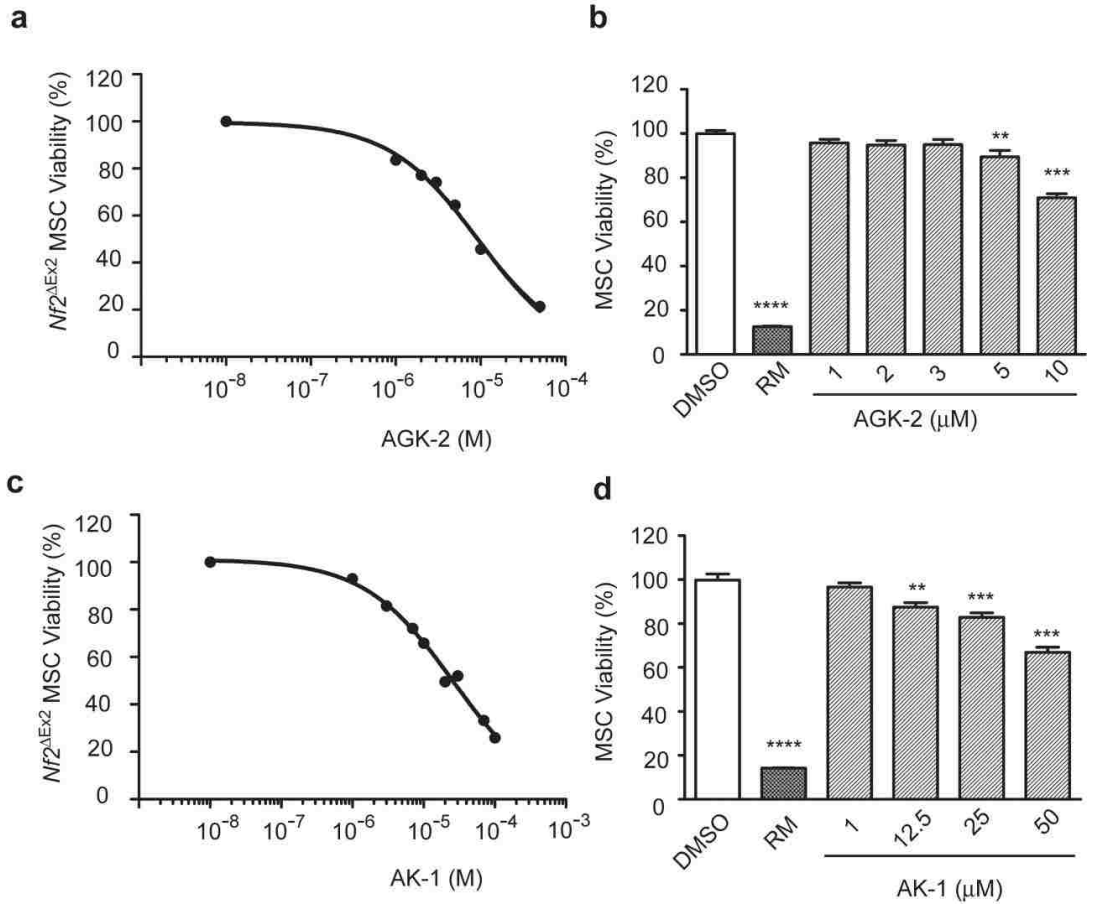

Figure 12. SIRT2 Inhibition with AGK2 and AK1 Selectively Decreases *Nf2*$^{\Delta Ex2}$ MSC Viability.

a) AGK2 dose response curve for cell viability. *Nf2*$^{\Delta Ex2}$ MSC were seeded at 5,000 cells/well in 384-well dishes and were incubated with increasing concentrations of AGK2 for 24 hours. Cell viability was assessed with the CellTiter-Fluor assay. DMSO control was considered 100% viability. Rapamycin (RM) (50 μM) was used as positive control for cell death. Graph represents the mean ± SEM of 3 independent experiments analyzed together (n=96), IC_{50}=9.01μM, log [inhibitor] vs. response, variable slope (four parameters). **b)** AGK2 dose response for control MSC viability. Cell viability was measured as in (a). Graph represents the mean ± SEM (n=36). ***P*<0.01; ****P*<0.001;*****P*<0.0001 determined by one-way ANOVA using Turkey's multiple comparison test. **c)** AK1 dose response curve for *Nf2*$^{\Delta Ex2}$ MSC viability. Cell viability assessed as in (a). Graph represents the mean ± SEM of 3 independent experiments analyzed together (n=96), IC_{50}=26.1μM, log [inhibitor] vs. response, variable slope (four parameters). **d)** AK1 dose viability response for control MSC. Cell viability was measured as in (a). Graph represents the mean ± SEM (n=20). ****P*<0.001; *****P*<0.0001 determined by one-way ANOVA using Turkey's multiple comparison test.

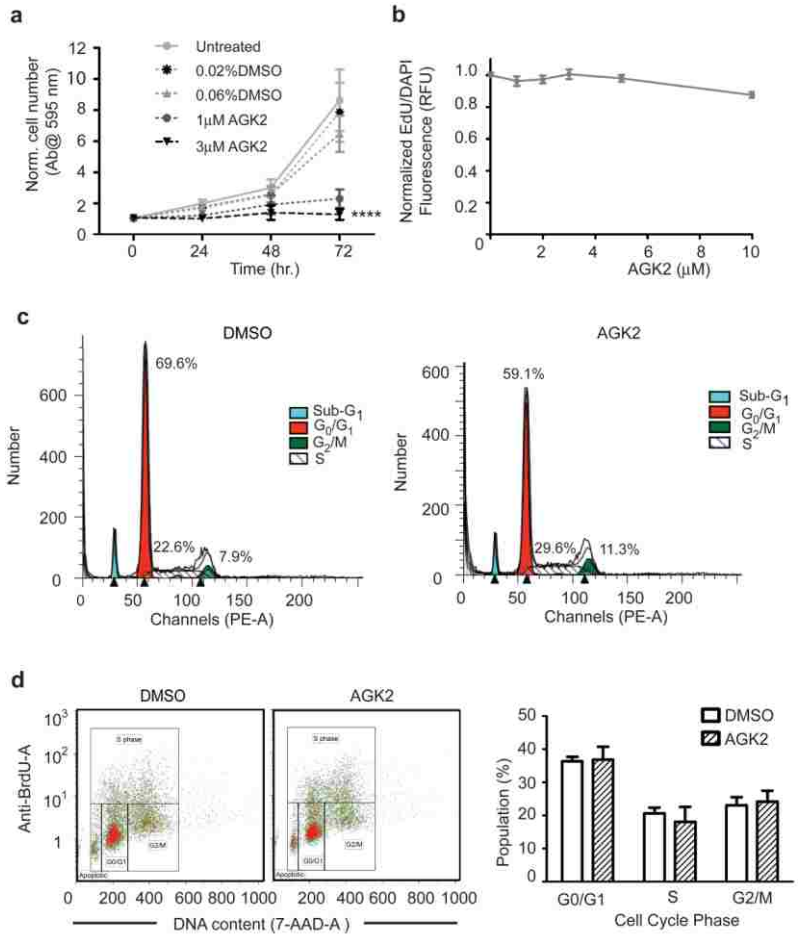

Figure 13. AGK2 Decreases *Nf2*$^{\Delta Ex2}$ MSC Proliferation without Interfering with Cell Cycle Progression.

a) *Nf2*$^{\Delta Ex2}$ MSC were incubated with AGK2 or DMSO for the indicated times and the number of cells was assessed using a crystal violet assay. Graph combines 3 independent experiments in triplicates (mean ± SEM, n=9). **b)** *Nf2*$^{\Delta Ex2}$ MSC were treated with increasing AGK2 concentrations for 24 hours. For the last 6 hours 10 μM EdU was added to the culture. Incorporation of EdU into S-phase cells was assessed with the EdU Click-It microplate assay. Graph combines 3 independent experiments (mean ± SEM, n=44). **c)** *Nf2*$^{\Delta Ex2}$ MSC were treated with 5 μM AGK2 for 8 hours prior to propidium iodide labeling. Cells were analyzed by flow cytometry and the diploid cell population was evaluated with the ModFit program. **d)** *Nf2*$^{\Delta Ex2}$ MSC were treated with AGK2 or DMSO control overnight and with 10 μM BrdU for the last 3 hr of incubation. Cells were analyzed by flow cytometry. Plot of the distribution of BrdU- and 7-AAD-labelled cells analyzed with Kaluza software. These distribution plots are representative of 3 independent experiments (n=3). Bar graph of the distribution of the cell cycle phases of the experiments as mean ± SEM.

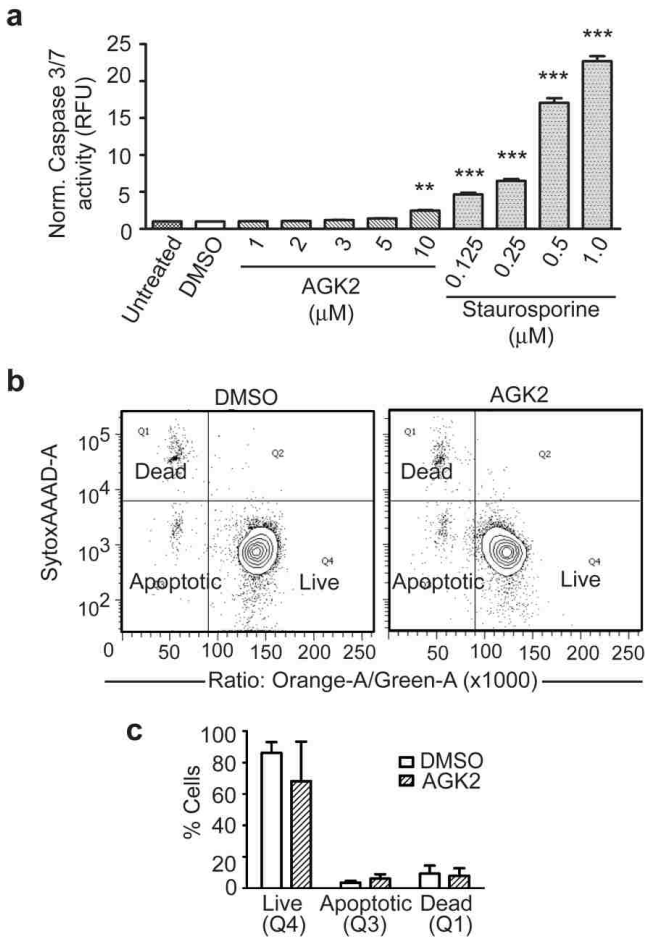

Figure 14. SIRT2 Inhibition with AGK2 Does Not Induce Significant Apoptosis.

a) Caspase 3/7 activity assay. *Nf2*$^{\Delta Ex2}$ MSC were seeded in 384 well plates at 5,000 cells/well in 20 µl phenol-red free medium. After 16 hours 5 µl/well of inhibitor/vehicle was added and incubated for an additional 8 hours. Activity of the Caspase 3/7 was measured with the ApoONE Homogeneous assay. Staurosporine curve was used as positive control. Histogram represents 3 independent experiments (n=96) normalized to untreated and analyzed together. ***P*<0.05; ****P*<0.001determined by one-way ANOVA using Dunnett's multiple comparison test to DMSO control. **b)** Plasma membrane asymmetry was evaluated with the Violet ratiometric assay by flow cytometry. *Nf2*$^{\Delta Ex2}$ MSC were incubated with AGK2 or DMSO vehicle for 24 hours and analyzed by flow cytometry. Densitometry graph: apoptotic (Q3), dead (Q1), live (Q4). Below, bar graph represents mean ± SEM of 3 independent experiments (n=3).

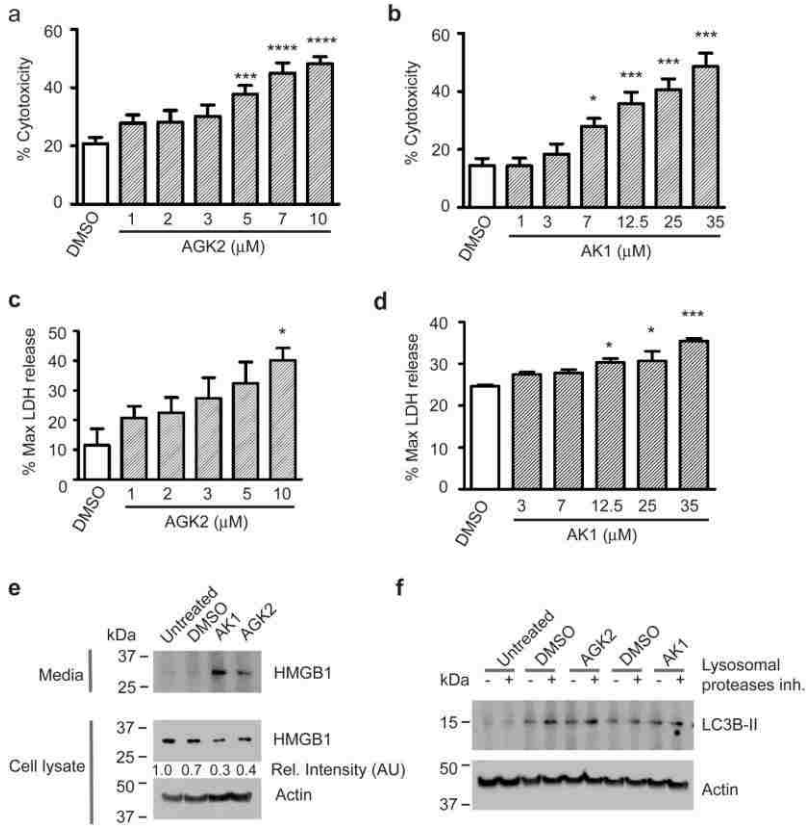

Figure 15. SIRT2 Inhibition Causes Release of LDH and HMGB1 from *Nf2*$^{\Delta Ex2}$ MSC.

Nf2$^{\Delta Ex2}$ MSC were seeded in 384 well-plates at 5,000 cell/well with cellTox-Green dye in phenol-red free medium. After attachment cells were treated with increasing concentrations of **a)** AGK2 and **b)** AK1 and incubated for 24 hours. Cytotoxicity was measure in a plate reader. Digitonin treatment was considered 100% cytotoxicity control. **P*<0.05; ****P*<0.001; *****P*<0.0001determined by one-way ANOVA using Bonferroni's multiple comparison test. **c)** *Nf2*$^{\Delta Ex2}$ MSC (5,000 cells/well in a 384-well plate) were treated for 4 hours with increasing concentrations of AGK2 and release of LDH into the medium was measured with a fluorogenic assay, the CytoTox-ONE homogenous membrane integrity assay in a plate reader; digitonin was considered as control for maximum LDH release. **P*<0.05 determined by one-way ANOVA using Dunnett's multiple comparison test **d)** Assessment of LDH released to the medium by *Nf2*$^{\Delta Ex2}$ MSC treated 4 hours with increasing concentrations of AK1 as in (c), **P*<0.05; ****P*<0.001 determined by one-way ANOVA using Dunnett's multiple comparison test. **e)** *Nf2*$^{\Delta Ex2}$ MSC were seeded in 6-well plates and treated for 6 hours with inhibitors/vehicle. HMGB1 release into the medium and cellular content of HMGB1 was assessed by western blot with anti-HMBG1 antibody. Anti-β-actin was used as loading control. **f)** Induction of autophagy was assessed by LC3B-II immunobloting. *Nf2*$^{\Delta Ex2}$ were treated for 3 hours with AGK2 or AK1 plus and minus 10 μg/ml acidic lysosomal proteases inhibitors (E64-d and pepstatin-A). Cell were lysed in 1% SDS buffer and resolved by western blot for anti-LC3B. Anti-β-actin was used as loading control.

CHAPTER FOUR: CONCLUSION

The results described in the previous chapters address an urgent need for effective NF2 therapy. The overall survival rate in NF2 patients estimated at 20 years from the diagnosis is 38%, but the consequences of the tumors greatly decrease the quality of life from diagnosis. Despite the identification of several potential targets by the investigation of causal molecular mechanisms of the tumorigenesis in *NF2* mutated cells, currently there is no drug indicated by the Food and Drug Administration (FDA) for NF2 therapy [109]. The work described in this dissertation validates two independent target enzymes, the LIM domain kinases, identified as downstream kinases of the Rac/Cdc42-PAK over-activated signaling pathway in *NF2* deficient schwannoma cells, and the SIRT2 deacetylase identified in an unbiased HTS of the LOPAC library.

Merlin's capability to act as a tumor suppressor was initially related to its ability to suppress Rac1 recruitment, preventing loss of contact inhibition associated with tumorigenesis [110]. We validated LIMK, a Rac1 pathway related downstream kinase as a target for NF2 therapeutics; inhibition of LIMK effectively decreased merlin-inactivated MSC proliferation by blocking the cell cycle progression at the G_2/M phase. Confocal microscopy showed that the LIMK inhibitor BMS-5 arrested cells at pro-metaphase by causing abnormal mitotic spindle and centrosome organization, two major effects molecularly linked and explained by the inhibition of the cofilin and aurora A phosphorylation. Therefore, the pharmacological inhibition of LIMK with BMS-5 falls in the category of chemotherapeutics with its mechanism of action being interference with cell division. Several cancer chemotherapies are based on the premise that

cancer/tumor cells proliferate at faster rate than the healthy cells, therefore drugs that interfere with cell proliferation have increased effect on cancer cells and offer a therapeutic window. However, other fast dividing cells such as cells in the bone marrow, digestive tract, and hair follicles are affected and cause side effects. The most common side effects are: decreased production of blood cells and immunosuppression [111], inflammation of the lining of the digestive tract accompanying nausea, vomiting, diarrhea and anorexia [112] and hair loss (alopecia) [113]. LIMK inhibitors might have similar side effects. Undoubtedly, more studies are needed to determine LIMK inhibitors systemic effect and if tumor cells will be able to develop resistance. Currently, LIMK inhibitors have only been tested topically to treat elevated optic pressure in glaucoma patients, which was reported using a specific LIMK2 inhibitor [114]. However the increasing knowledge of their involvement in various cancers placed LIMK as emerging cancer targets. Hence, pharmaceutical companies and researchers are developing new highly potent and specific candidate drugs that may prove valuable for the treatment of NF2. Despite the benign nature of the NF2-related tumors, *NF2* deficient cells share major characteristics of cancer cells making it appealing to test new cancer therapies in NF2-related tumors. Cancer and NF2 tumor cells present sustainability of proliferative signaling, defense against cell death, ability to silence growth suppressors, replicative immortality, stimulation of angiogenesis, reprogramming of energetic metabolism and evasion of immune attack, whereas the main difference is that NF2 tumors do not invade other tissues or metastasize [115].

Contrary to the classical cell-cycle related kinases, SIRT2 is a more recent class of target enzyme uncovered in the tumorigenesis field. Chronologically, the sirtuin family came to light when research identified these enzymes as regulators of lifespan in the yeast *Saccharomyces cerevisiae* [116, 117]. In mammals, SIRT1 was the first one discovered 13 years ago and has been the most extensively studied, and it is related to metabolic regulation; since then, seven sirtuins were discovered. Identification of SIRT2 led to a vast number of publications that shed light on its function [118]. The involvement of SIRT2 in cancer/tumors is currently unclear and seems to be heavily dependent on the molecular pathways de-regulated in different tumors. Moreover, plenty remains to be elucidated about the sirtuins biology. The appeal of a new therapeutic avenue keeps the scientific field working relentlessly to identify more specific and potent SIRT2 inhibitors to study their effect on tumor growth. Based on our studies, SIRT2 inhibitors such as AGK2 and AK1, contrary to LIMK inhibitors, fall into a different chemotherapeutical mechanism of action, drugs that induce tumor cell death.

A classic chemotherapy principle is that combinatorial regimens provide maximum benefits because treatments with two drugs within their therapeutic dose range afflict a maximum tumor cytotoxic effect with minimum systemic toxicity. Additionally, because the tumor might have a heterogeneous cell population, two compounds with independent targets improve the chances to prevent or slow the rise of a drug-resistant subpopulation. It is recommended to combine compounds with different mechanism of action because it leads to a synergic effect on tumor cells with minimum general toxicity [119]. Therefore, the LIMK inhibitors cell cycle interference and the

SIRT2 inhibitors tumor cell death are two types of drugs that might be of a benefit to combine. Not only the mechanisms of action are different, one drug halts cell division and the other kills tumor cells, but also their targets are completely independent, in pathways and enzymatic activity. One drug affects the phosphorylation status of proteins and the other drug affects their acetylation status. As of today, LIMK and SIRT2 inhibitors still need to be tested in pre-clinical and clinical studies before formulating conclusions on their therapeutic use or potentiality as combinatorial drugs for NF2 and *NF2* mutation-related tumors.

To conclude, this dissertation presents to the NF2 field the validation of two potential drug targets. Further research is needed to determine the clinical value through *in vivo* pre-clinical testing and clinical trials.

APPENDIX A: CHAPTER TWO SUPPLEMENTARY FIGURES

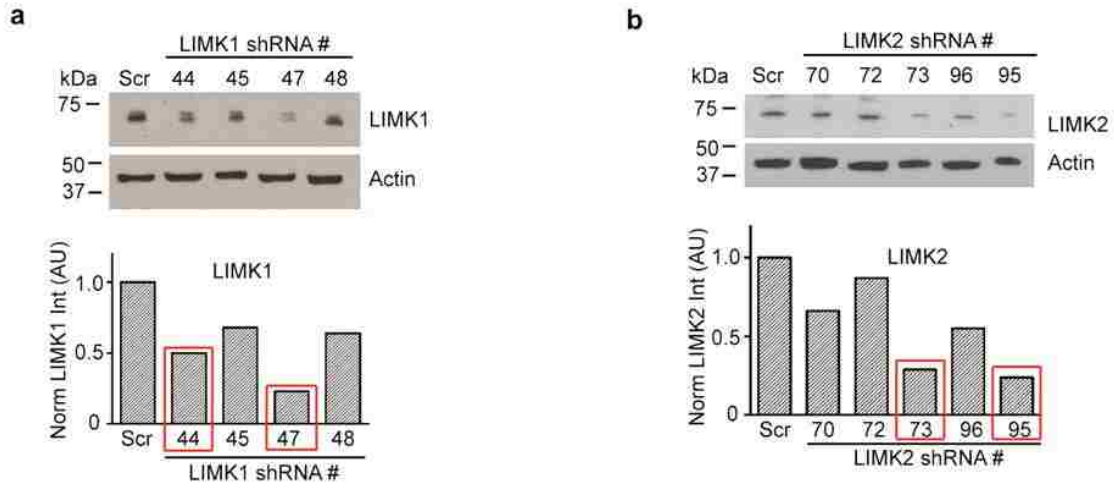

Supplementary Figure 1. Effective LIMK Knockdown.

Nf2$^{\Delta Ex2}$ MSCs were transduced with lentiviral vectors with various shRNA constructs targeting LIMK1 and LIMK 2. Western blotting of *Nf2*$^{\Delta Ex2}$ MSC whole cell extracts treated with scrambled shRNA control and various constructs targeting LIMK1 **(a)** and LIMK2 **(b)**. Plots of densitometry analysis of the immunoblots by ImageJ software are shown below each panel. The red rectangles mark the constructs chosen for the experiments.

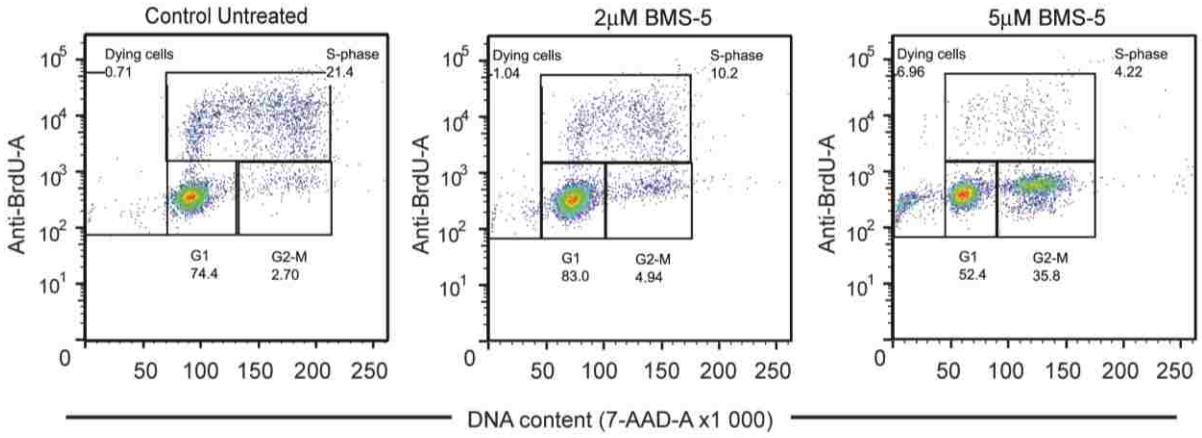

Supplementary Figure 2. Inhibition of LIMK with BMS-5 Interferes with *Nf2*$^{\Delta Ex2}$ MSCs Cell Cycle Progression in a Dose-Dependent Manner.

Nf2$^{\Delta Ex2}$ MSCs were grown in a 6-well format and treated for 24 hrs with 2 and 5 μM BMS-5 prior to 3 hr BrdU labeling and analysis by flow cytometry with a BD Cantos II flow cytometer controlled by BD FACSDiva™ 6.1.3 software. Distribution of BrdU- and 7-AAD-labelled cells into dying cells, G_0/G_1, S, and G_2/M phase was analyzed with FlowJo software. At higher BMS-5 dose *Nf2*$^{\Delta Ex2}$ MSCs were trapped in higher proportion in the G_2/M phase and evidenced a decrease in the number of cells in S phase.

APPENDIX B: CHAPTER THREE SUPPLEMENTARY FIGURE

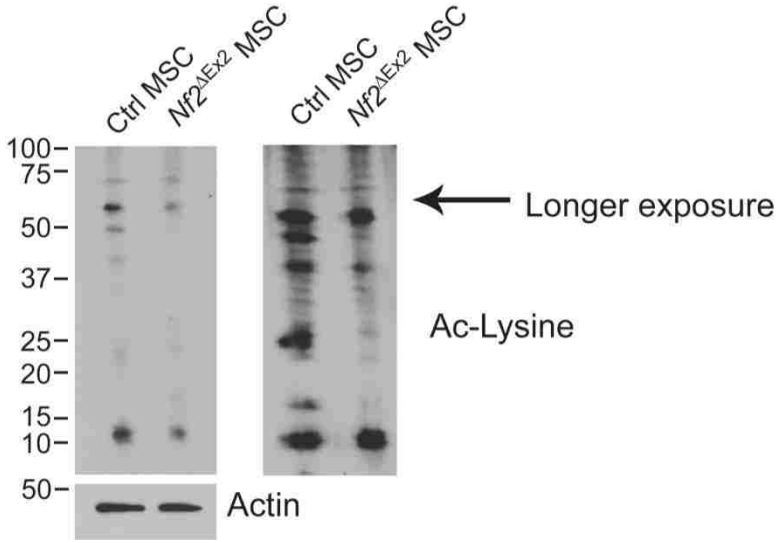

Supplementary Figure 3. *Nf2*$^{\Delta Ex2}$ MSC have Lower Levels of Lysine Acetylation Compared to Control MSC.

Cell lysates of control *Nf2*$^{flox2/flox2}$ MSC and *Nf2*$^{\Delta Ex2}$ MSC were analyzed by western blotting for acetyl-lysine; β-actin was used as loading control. The right panel shows a longer exposure of the blot and reveals multiple differentially acetylated bands.

REFERENCES

1. Asthagiri, A. R., Parry, D. M., Butman, J. A., Kim, H. J., Tsilou, E. T., Zhuang, Z. & Lonser, R. R. (2009) Neurofibromatosis type 2, *Lancet.* **373**, 1974-86.

2. Evans, D. G. (2009) Neurofibromatosis type 2 (NF2): a clinical and molecular review, *Orphanet journal of rare diseases.* **4**, 16.

3. Ferner, R. E. (2007) Neurofibromatosis 1 and neurofibromatosis 2: a twenty first century perspective, *Lancet Neurol.* **6**, 340-51.

4. Rouleau, G. A., Merel, P., Lutchman, M., Sanson, M., Zucman, J., Marineau, C., Hoang-Xuan, K., Demczuk, S., Desmaze, C., Plougastel, B. & et al. (1993) Alteration in a new gene encoding a putative membrane-organizing protein causes neuro-fibromatosis type 2, *Nature.* **363**, 515-21.

5. Zhang, N., Bai, H., David, K. K., Dong, J., Zheng, Y., Cai, J., Giovannini, M., Liu, P., Anders, R. A. & Pan, D. (2010) The Merlin/NF2 tumor suppressor functions through the YAP oncoprotein to regulate tissue homeostasis in mammals, *Dev Cell.* **19**, 27-38.

6. Striedinger, K., VandenBerg, S. R., Baia, G. S., McDermott, M. W., Gutmann, D. H. & Lal, A. (2008) The neurofibromatosis 2 tumor suppressor gene product, merlin, regulates human meningioma cell growth by signaling through YAP, *Neoplasia.* **10**, 1204-12.

7. Stamenkovic, I. & Yu, Q. (2010) Merlin, a "magic" linker between extracellular cues and intracellular signaling pathways that regulate cell motility, proliferation, and survival, *Current protein & peptide science.* **11**, 471-84.

8. Thaxton, C., Lopera, J., Bott, M. & Fernandez-Valle, C. (2008) Neuregulin and laminin stimulate phosphorylation of the NF2 tumor suppressor in Schwann cells by distinct protein kinase A and p21-activated kinase-dependent pathways, *Oncogene.* **27**, 2705-15.

9. James, M. F., Han, S., Polizzano, C., Plotkin, S. R., Manning, B. D., Stemmer-Rachamimov, A. O., Gusella, J. F. & Ramesh, V. (2009) NF2/merlin is a novel negative regulator of mTOR complex 1, and activation of mTORC1 is associated with meningioma and schwannoma growth, *Mol Cell Biol.* **29**, 4250-61.

10. Li, W., Chong, H. & Guan, K. L. (2001) Function of the Rho family GTPases in Ras-stimulated Raf activation, *The Journal of biological chemistry.* **276**, 34728-37.

11. Li, W., You, L., Cooper, J., Schiavon, G., Pepe-Caprio, A., Zhou, L., Ishii, R., Giovannini, M., Hanemann, C. O., Long, S. B., Erdjument-Bromage, H., Zhou, P., Tempst, P. & Giancotti, F. G. (2010) Merlin/NF2 suppresses tumorigenesis by inhibiting the E3 ubiquitin ligase CRL4(DCAF1) in the nucleus, *Cell.* **140**, 477-90.

12. Kissil, J. L., Wilker, E. W., Johnson, K. C., Eckman, M. S., Yaffe, M. B. & Jacks, T. (2003) Merlin, the product of the Nf2 tumor suppressor gene, is an inhibitor of the p21-activated kinase, Pak1, *Mol Cell.* **12**, 841-9.

13. Xiao, G. H., Beeser, A., Chernoff, J. & Testa, J. R. (2002) p21-activated kinase links Rac/Cdc42 signaling to merlin, *The Journal of biological chemistry.* **277**, 883-6.

14. Kaempchen, K., Mielke, K., Utermark, T., Langmesser, S. & Hanemann, C. O. (2003) Upregulation of the Rac1/JNK signaling pathway in primary human schwannoma cells, *Human molecular genetics.* **12**, 1211-21.

15. Yi, C., Wilker, E. W., Yaffe, M. B., Stemmer-Rachamimov, A. & Kissil, J. L. (2008) Validation of the p21-activated kinases as targets for inhibition in neurofibromatosis type 2, *Cancer research.* **68**, 7932-7.

16. Scott, R. W. & Olson, M. F. (2007) LIM kinases: function, regulation and association with human disease, *J Mol Med (Berl).* **85**, 555-68.

17. Manetti, F. (2012) LIM kinases are attractive targets with many macromolecular partners and only a few small molecule regulators, *Med Res Rev.* **32**, 968-98.

18. Lim, M. K., Kawamura, T., Ohsawa, Y., Ohtsubo, M., Asakawa, S., Takayanagi, A. & Shimizu, N. (2007) Parkin interacts with LIM Kinase 1 and reduces its cofilin-phosphorylation activity via ubiquitination, *Exp Cell Res.* **313**, 2858-74.

19. Soosairajah, J., Maiti, S., Wiggan, O., Sarmiere, P., Moussi, N., Sarcevic, B., Sampath, R., Bamburg, J. R. & Bernard, O. (2005) Interplay between components of a novel LIM kinase-slingshot phosphatase complex regulates cofilin, *EMBO J.* **24**, 473-86.

20. Tursun, B., Schluter, A., Peters, M. A., Viehweger, B., Ostendorff, H. P., Soosairajah, J., Drung, A., Bossenz, M., Johnsen, S. A., Schweizer, M., Bernard, O. & Bach, I. (2005) The ubiquitin ligase Rnf6 regulates local LIM kinase 1 levels in axonal growth cones, *Genes & development.* **19**, 2307-19.

21. Yang, N., Higuchi, O., Ohashi, K., Nagata, K., Wada, A., Kangawa, K., Nishida, E. & Mizuno, K. (1998) Cofilin phosphorylation by LIM-kinase 1 and its role in Rac-mediated actin reorganization, *Nature.* **393**, 809-12.

22. Yang, E. J., Yoon, J. H., Min, D. S. & Chung, K. C. (2004) LIM kinase 1 activates cAMP-responsive element-binding protein during the neuronal differentiation of immortalized hippocampal progenitor cells, *The Journal of biological chemistry.* **279**, 8903-10.

23. Sacchetti, P., Carpentier, R., Segard, P., Olive-Cren, C. & Lefebvre, P. (2006) Multiple signaling pathways regulate the transcriptional activity of the orphan nuclear receptor NURR1, *Nucleic acids research.* **34**, 5515-27.

24. Ritchey, L., Ottman, R., Roumanos, M. & Chakrabarti, R. (2012) A functional cooperativity between Aurora A kinase and LIM kinase1: implication in the mitotic process, *Cell Cycle.* **11**, 296-309.

25. Johnson, E. O., Chang, K. H., Ghosh, S., Venkatesh, C., Giger, K., Low, P. S. & Shah, K. (2012) LIMK2 is a crucial regulator and effector of Aurora-A-kinase-mediated malignancy, *J Cell Sci.* **125**, 1204-16.

26. Meng, Y., Zhang, Y., Tregoubov, V., Janus, C., Cruz, L., Jackson, M., Lu, W. Y., MacDonald, J. F., Wang, J. Y., Falls, D. L. & Jia, Z. (2002) Abnormal spine morphology and enhanced LTP in LIMK-1 knockout mice, *Neuron.* **35**, 121-33.

27. Meng, Y., Takahashi, H., Meng, J., Zhang, Y., Lu, G., Asrar, S., Nakamura, T. & Jia, Z. (2004) Regulation of ADF/cofilin phosphorylation and synaptic function by LIM-kinase, *Neuropharmacology.* **47**, 746-54.

28. Amano, T., Kaji, N., Ohashi, K. & Mizuno, K. (2002) Mitosis-specific activation of LIM motif-containing protein kinase and roles of cofilin phosphorylation and dephosphorylation in mitosis, *The Journal of biological chemistry.* **277**, 22093-102.

29. Sumi, T., Hashigasako, A., Matsumoto, K. & Nakamura, T. (2006) Different activity regulation and subcellular localization of LIMK1 and LIMK2 during cell cycle transition, *Exp Cell Res.* **312**, 1021-30.

30. Sumi, T., Matsumoto, K. & Nakamura, T. (2002) Mitosis-dependent phosphorylation and activation of LIM-kinase 1, *Biochemical and biophysical research communications.* **290**, 1315-20.

31. Barr, A. R. & Gergely, F. (2007) Aurora-A: the maker and breaker of spindle poles, *J Cell Sci.* **120**, 2987-96.

32. Nikonova, A. S., Astsaturov, I., Serebriiskii, I. G., Dunbrack, R. L., Jr. & Golemis, E. A. (2013) Aurora A kinase (AURKA) in normal and pathological cell division, *Cellular and molecular life sciences : CMLS.* **70**, 661-87.

33. Acevedo, K., Moussi, N., Li, R., Soo, P. & Bernard, O. (2006) LIM kinase 2 is widely expressed in all tissues, *J Histochem Cytochem.* **54**, 487-501.

34. Foletta, V. C., Lim, M. A., Soosairajah, J., Kelly, A. P., Stanley, E. G., Shannon, M., He, W., Das, S., Massague, J. & Bernard, O. (2003) Direct signaling by the BMP type II receptor via the cytoskeletal regulator LIMK1, *J Cell Biol.* **162**, 1089-98.

35. Linthicum, F. H., Jr., Saleh, E. S., Hitselberger, W. E., Brackmann, D. E. & Hung, G. (2002) Growth of postoperative remnants of unilateral vestibular nerve schwannoma: role of the vestibular ganglion, *ORL; journal for oto-rhino-laryngology and its related specialties.* **64**, 138-42.

36. Bagheri-Yarmand, R., Mazumdar, A., Sahin, A. A. & Kumar, R. (2006) LIM kinase 1 increases tumor metastasis of human breast cancer cells via regulation of the urokinase-type plasminogen activator system, *Int J Cancer.* **118**, 2703-10.

37. Horita, Y., Ohashi, K., Mukai, M., Inoue, M. & Mizuno, K. (2008) Suppression of the invasive capacity of rat ascites hepatoma cells by knockdown of Slingshot or LIM kinase, *The Journal of biological chemistry.* **283**, 6013-21.

38. McConnell, B. V., Koto, K. & Gutierrez-Hartmann, A. (2011) Nuclear and cytoplasmic LIMK1 enhances human breast cancer progression, *Mol Cancer.* **10**, 75.

39. Okamoto, I., Pirker, C., Bilban, M., Berger, W., Losert, D., Marosi, C., Haas, O. A., Wolff, K. & Pehamberger, H. (2005) Seven novel and stable translocations associated with oncogenic gene expression in malignant melanoma, *Neoplasia.* **7**, 303-11.

40. Manetti, F. (2012) Recent findings confirm LIM domain kinases as emerging target candidates for cancer therapy, *Curr Cancer Drug Targets.* **12**, 543-60.

41. Choudhary, C., Kumar, C., Gnad, F., Nielsen, M. L., Rehman, M., Walther, T. C., Olsen, J. V. & Mann, M. (2009) Lysine acetylation targets protein complexes and co-regulates major cellular functions, *Science.* **325**, 834-40.

42. Dokmanovic, M., Clarke, C. & Marks, P. A. (2007) Histone deacetylase inhibitors: overview and perspectives, *Molecular cancer research : MCR.* **5**, 981-9.

43. Michishita, E., Park, J. Y., Burneskis, J. M., Barrett, J. C. & Horikawa, I. (2005) Evolutionarily conserved and nonconserved cellular localizations and functions of human SIRT proteins, *Molecular biology of the cell.* **16**, 4623-35.

44. North, B. J. & Verdin, E. (2004) Sirtuins: Sir2-related NAD-dependent protein deacetylases, *Genome biology.* **5**, 224.

45. North, B. J., Marshall, B. L., Borra, M. T., Denu, J. M. & Verdin, E. (2003) The human Sir2 ortholog, SIRT2, is an NAD+-dependent tubulin deacetylase, *Mol Cell.* **11**, 437-44.

46. Hubbert, C., Guardiola, A., Shao, R., Kawaguchi, Y., Ito, A., Nixon, A., Yoshida, M., Wang, X. F. & Yao, T. P. (2002) HDAC6 is a microtubule-associated deacetylase, *Nature.* **417**, 455-8.

47. Jing, E., Gesta, S. & Kahn, C. R. (2007) SIRT2 regulates adipocyte differentiation through FoxO1 acetylation/deacetylation, *Cell metabolism.* **6**, 105-14.

48. Ji, S., Doucette, J. R. & Nazarali, A. J. (2011) Sirt2 is a novel in vivo downstream target of Nkx2.2 and enhances oligodendroglial cell differentiation, *Journal of molecular cell biology.* **3**, 351-9.

49. Li, W., Zhang, B., Tang, J., Cao, Q., Wu, Y., Wu, C., Guo, J., Ling, E. A. & Liang, F. (2007) Sirtuin 2, a mammalian homolog of yeast silent information regulator-2 longevity regulator, is an oligodendroglial protein that decelerates cell differentiation through deacetylating alpha-tubulin, *The Journal of neuroscience : the official journal of the Society for Neuroscience.* **27**, 2606-16.

50. Beirowski, B., Gustin, J., Armour, S. M., Yamamoto, H., Viader, A., North, B. J., Michan, S., Baloh, R. H., Golden, J. P., Schmidt, R. E., Sinclair, D. A., Auwerx, J. & Milbrandt, J. (2011) Sir-two-homolog 2 (Sirt2) modulates peripheral myelination through polarity protein Par-3/atypical protein kinase C (aPKC) signaling, *Proceedings of the National Academy of Sciences of the United States of America.* **108**, E952-61.

51. Outeiro, T. F., Kontopoulos, E., Altmann, S. M., Kufareva, I., Strathearn, K. E., Amore, A. M., Volk, C. B., Maxwell, M. M., Rochet, J. C., McLean, P. J., Young, A. B., Abagyan, R., Feany, M. B., Hyman, B. T. & Kazantsev, A. G. (2007) Sirtuin 2 inhibitors rescue alpha-synuclein-mediated toxicity in models of Parkinson's disease, *Science.* **317**, 516-9.

52. Liu, L., Arun, A., Ellis, L., Peritore, C. & Donmez, G. (2012) Sirtuin 2 (SIRT2) enhances 1-methyl-4-phenyl-1,2,3,6-tetrahydropyridine (MPTP)-induced nigrostriatal damage via deacetylating forkhead box O3a (Foxo3a) and activating Bim protein, *The Journal of biological chemistry.* **287**, 32307-11.

53. Chopra, V., Quinti, L., Kim, J., Vollor, L., Narayanan, K. L., Edgerly, C., Cipicchio, P. M., Lauver, M. A., Choi, S. H., Silverman, R. B., Ferrante, R. J., Hersch, S. &

Kazantsev, A. G. (2012) The sirtuin 2 inhibitor AK-7 is neuroprotective in Huntington's disease mouse models, *Cell reports.* **2**, 1492-7.

54. Inoue, T., Nakayama, Y., Yamada, H., Li, Y. C., Yamaguchi, S., Osaki, M., Kurimasa, A., Hiratsuka, M., Katoh, M. & Oshimura, M. (2009) SIRT2 downregulation confers resistance to microtubule inhibitors by prolonging chronic mitotic arrest, *Cell Cycle.* **8**, 1279-91.

55. Dryden, S. C., Nahhas, F. A., Nowak, J. E., Goustin, A. S. & Tainsky, M. A. (2003) Role for human SIRT2 NAD-dependent deacetylase activity in control of mitotic exit in the cell cycle, *Mol Cell Biol.* **23**, 3173-85.

56. North, B. J. & Verdin, E. (2007) Mitotic regulation of SIRT2 by cyclin-dependent kinase 1-dependent phosphorylation, *The Journal of biological chemistry.* **282**, 19546-55.

57. Pandithage, R., Lilischkis, R., Harting, K., Wolf, A., Jedamzik, B., Luscher-Firzlaff, J., Vervoorts, J., Lasonder, E., Kremmer, E., Knoll, B. & Luscher, B. (2008) The regulation of SIRT2 function by cyclin-dependent kinases affects cell motility, *J Cell Biol.* **180**, 915-29.

58. Kim, H. S., Vassilopoulos, A., Wang, R. H., Lahusen, T., Xiao, Z., Xu, X., Li, C., Veenstra, T. D., Li, B., Yu, H., Ji, J., Wang, X. W., Park, S. H., Cha, Y. I., Gius, D. & Deng, C. X. (2011) SIRT2 maintains genome integrity and suppresses tumorigenesis through regulating APC/C activity, *Cancer cell.* **20**, 487-99.

59. Heltweg, B., Gatbonton, T., Schuler, A. D., Posakony, J., Li, H., Goehle, S., Kollipara, R., Depinho, R. A., Gu, Y., Simon, J. A. & Bedalov, A. (2006) Antitumor activity of a small-molecule inhibitor of human silent information regulator 2 enzymes, *Cancer research.* **66**, 4368-77.

60. Vaquero, A., Scher, M. B., Lee, D. H., Sutton, A., Cheng, H. L., Alt, F. W., Serrano, L., Sternglanz, R. & Reinberg, D. (2006) SirT2 is a histone deacetylase with preference for histone H4 Lys 16 during mitosis, *Genes & development.* **20**, 1256-61.

61. Yang, M. H., Laurent, G., Bause, A. S., Spang, R., German, N., Haigis, M. C. & Haigis, K. M. (2013) HDAC6 and SIRT2 Regulate the Acetylation State and Oncogenic Activity of Mutant K-RAS, *Molecular cancer research : MCR.* **11**, 1072-7.

62. Liu, P. Y., Xu, N., Malyukova, A., Scarlett, C. J., Sun, Y. T., Zhang, X. D., Ling, D., Su, S. P., Nelson, C., Chang, D. K., Koach, J., Tee, A. E., Haber, M., Norris, M. D., Toon, C., Rooman, I., Xue, C., Cheung, B. B., Kumar, S., Marshall, G. M.,

Biankin, A. V. & Liu, T. (2013) The histone deacetylase SIRT2 stabilizes Myc oncoproteins, *Cell death and differentiation.* **20**, 503-14.

63. He, X., Nie, H., Hong, Y., Sheng, C., Xia, W. & Ying, W. (2012) SIRT2 activity is required for the survival of C6 glioma cells, *Biochemical and biophysical research communications.* **417**, 468-72.

64. Hiratsuka, M., Inoue, T., Toda, T., Kimura, N., Shirayoshi, Y., Kamitani, H., Watanabe, T., Ohama, E., Tahimic, C. G., Kurimasa, A. & Oshimura, M. (2003) Proteomics-based identification of differentially expressed genes in human gliomas: down-regulation of SIRT2 gene, *Biochemical and biophysical research communications.* **309**, 558-66.

65. Zhang, Y., Au, Q., Zhang, M., Barber, J. R., Ng, S. C. & Zhang, B. (2009) Identification of a small molecule SIRT2 inhibitor with selective tumor cytotoxicity, *Biochemical and biophysical research communications.* **386**, 729-33.

66. Li, Y., Nie, H., Wu, D., Zhang, J., Wei, X. & Ying, W. (2013) Poly(ADP-ribose) polymerase mediates both cell death and ATP decreases in SIRT2 inhibitor AGK2-treated microglial BV2 cells, *Neuroscience letters.* **544**, 36-40.

67. Narayan, N., Lee, I. H., Borenstein, R., Sun, J., Wong, R., Tong, G., Fergusson, M. M., Liu, J., Rovira, II, Cheng, H. L., Wang, G., Gucek, M., Lombard, D., Alt, F. W., Sack, M. N., Murphy, E., Cao, L. & Finkel, T. (2012) The NAD-dependent deacetylase SIRT2 is required for programmed necrosis, *Nature.* **492**, 199-204.

68. de Oliveira, R. M., Sarkander, J., Kazantsev, A. G. & Outeiro, T. F. (2012) SIRT2 as a Therapeutic Target for Age-Related Disorders, *Frontiers in pharmacology.* **3**, 82.

69. Moniot, S., Schutkowski, M. & Steegborn, C. (2013) Crystal structure analysis of human Sirt2 and its ADP-ribose complex, *Journal of structural biology.* **182**, 136-43.

70. Baser, M. E., De Rienzo, A., Altomare, D., Balsara, B. R., Hedrick, N. M., Gutmann, D. H., Pitts, L. H., Jackler, R. K. & Testa, J. R. (2002) Neurofibromatosis 2 and malignant mesothelioma, *Neurology.* **59**, 290-1.

71. Kalamarides, M., Acosta, M. T., Babovic-Vuksanovic, D., Carpen, O., Cichowski, K., Evans, D. G., Giancotti, F., Hanemann, C. O., Ingram, D., Lloyd, A. C., Mayes, D. A., Messiaen, L., Morrison, H., North, K., Packer, R., Pan, D., Stemmer-Rachamimov, A., Upadhyaya, M., Viskochil, D., Wallace, M. R., Hunter-Schaedle, K. & Ratner, N. (2012) Neurofibromatosis 2011: a report of the

Children's Tumor Foundation annual meeting, *Acta neuropathologica.* **123**, 369-80.

72. Li, W., Cooper, J., Karajannis, M. A. & Giancotti, F. G. (2012) Merlin: a tumour suppressor with functions at the cell cortex and in the nucleus, *EMBO reports.* **13**, 204-15.

73. Pelton, P. D., Sherman, L. S., Rizvi, T. A., Marchionni, M. A., Wood, P., Friedman, R. A. & Ratner, N. (1998) Ruffling membrane, stress fiber, cell spreading and proliferation abnormalities in human Schwannoma cells, *Oncogene.* **17**, 2195-209.

74. Kissil, J. L., Johnson, K. C., Eckman, M. S. & Jacks, T. (2002) Merlin phosphorylation by p21-activated kinase 2 and effects of phosphorylation on merlin localization, *The Journal of biological chemistry.* **277**, 10394-9.

75. Shaw, R. J., Paez, J. G., Curto, M., Yaktine, A., Pruitt, W. M., Saotome, I., O'Bryan, J. P., Gupta, V., Ratner, N., Der, C. J., Jacks, T. & McClatchey, A. I. (2001) The Nf2 tumor suppressor, merlin, functions in Rac-dependent signaling, *Dev Cell.* **1**, 63-72.

76. Nakai, Y., Zheng, Y., MacCollin, M. & Ratner, N. (2006) Temporal control of Rac in Schwann cell-axon interaction is disrupted in NF2-mutant schwannoma cells, *The Journal of neuroscience : the official journal of the Society for Neuroscience.* **26**, 3390-5.

77. Goyal, P., Pandey, D., Behring, A. & Siess, W. (2005) Inhibition of nuclear import of LIMK2 in endothelial cells by protein kinase C-dependent phosphorylation at Ser-283, *The Journal of biological chemistry.* **280**, 27569-77.

78. Kaji, N., Muramoto, A. & Mizuno, K. (2008) LIM kinase-mediated cofilin phosphorylation during mitosis is required for precise spindle positioning, *The Journal of biological chemistry.* **283**, 4983-92.

79. Po'uha, S. T., Shum, M. S., Goebel, A., Bernard, O. & Kavallaris, M. (2010) LIM-kinase 2, a regulator of actin dynamics, is involved in mitotic spindle integrity and sensitivity to microtubule-destabilizing drugs, *Oncogene.* **29**, 597-607.

80. Yokoo, T., Toyoshima, H., Miura, M., Wang, Y., Iida, K. T., Suzuki, H., Sone, H., Shimano, H., Gotoda, T., Nishimori, S., Tanaka, K. & Yamada, N. (2003) p57Kip2 regulates actin dynamics by binding and translocating LIM-kinase 1 to the nucleus, *The Journal of biological chemistry.* **278**, 52919-23.

81. Thaxton, C., Bott, M., Walker, B., Sparrow, N. A., Lambert, S. & Fernandez-Valle, C. (2011) Schwannomin/merlin promotes Schwann cell elongation and influences myelin segment length, *Molecular and cellular neurosciences.* **47**, 1-9.

82. Iacovelli, J., Lopera, J., Bott, M., Baldwin, E., Khaled, A., Uddin, N. & Fernandez-Valle, C. (2007) Serum and forskolin cooperate to promote G1 progression in Schwann cells by differentially regulating cyclin D1, cyclin E1, and p27Kip expression, *Glia.* **55**, 1638-47.

83. Giovannini, M., Robanus-Maandag, E., van der Valk, M., Niwa-Kawakita, M., Abramowski, V., Goutebroze, L., Woodruff, J. M., Berns, A. & Thomas, G. (2000) Conditional biallelic Nf2 mutation in the mouse promotes manifestations of human neurofibromatosis type 2, *Genes & development.* **14**, 1617-30.

84. Ross-Macdonald, P., de Silva, H., Guo, Q., Xiao, H., Hung, C. Y., Penhallow, B., Markwalder, J., He, L., Attar, R. M., Lin, T. A., Seitz, S., Tilford, C., Wardwell-Swanson, J. & Jackson, D. (2008) Identification of a nonkinase target mediating cytotoxicity of novel kinase inhibitors, *Mol Cancer Ther.* **7**, 3490-8.

85. Hung, G., Li, X., Faudoa, R., Xeu, Z., Kluwe, L., Rhim, J. S., Slattery, W. & Lim, D. (2002) Establishment and characterization of a schwannoma cell line from a patient with neurofibromatosis 2, *International journal of oncology.* **20**, 475-82.

86. Arber, S., Barbayannis, F. A., Hanser, H., Schneider, C., Stanyon, C. A., Bernard, O. & Caroni, P. (1998) Regulation of actin dynamics through phosphorylation of cofilin by LIM-kinase, *Nature.* **393**, 805-9.

87. Bashour, A. M., Meng, J. J., Ip, W., MacCollin, M. & Ratner, N. (2002) The neurofibromatosis type 2 gene product, merlin, reverses the F-actin cytoskeletal defects in primary human Schwannoma cells, *Mol Cell Biol.* **22**, 1150-7.

88. Sparrow, N., Manetti, M. E., Bott, M., Fabianac, T., Petrilli, A., Bates, M. L., Bunge, M. B., Lambert, S. & Fernandez-Valle, C. (2012) The actin-severing protein cofilin is downstream of neuregulin signaling and is essential for Schwann cell myelination, *The Journal of neuroscience : the official journal of the Society for Neuroscience.* **32**, 5284-97.

89. Cote, M. C., Lavoie, J. R., Houle, F., Poirier, A., Rousseau, S. & Huot, J. (2010) Regulation of vascular endothelial growth factor-induced endothelial cell migration by LIM kinase 1-mediated phosphorylation of annexin 1, *The Journal of biological chemistry.* **285**, 8013-21.

90. Plotkin, S. R., Stemmer-Rachamimov, A. O., Barker, F. G., 2nd, Halpin, C., Padera, T. P., Tyrrell, A., Sorensen, A. G., Jain, R. K. & di Tomaso, E. (2009) Hearing

improvement after bevacizumab in patients with neurofibromatosis type 2, *N Engl J Med.* **361**, 358-67.

91. Fong, B., Barkhoudarian, G., Pezeshkian, P., Parsa, A. T., Gopen, Q. & Yang, I. (2011) The molecular biology and novel treatments of vestibular schwannomas, *Journal of neurosurgery.* **115**, 906-14.

92. Hawse, W. F., Hoff, K. G., Fatkins, D. G., Daines, A., Zubkova, O. V., Schramm, V. L., Zheng, W. & Wolberger, C. (2008) Structural insights into intermediate steps in the Sir2 deacetylation reaction, *Structure.* **16**, 1368-77.

93. Petrilli, A., Copik, A., Posadas, M., Chang, L. S., Welling, D. B., Giovannini, M. & Fernandez-Valle, C. (2013) LIM domain kinases as potential therapeutic targets for neurofibromatosis type 2, *Oncogene*.

94. Kroemer, G., Galluzzi, L., Vandenabeele, P., Abrams, J., Alnemri, E. S., Baehrecke, E. H., Blagosklonny, M. V., El-Deiry, W. S., Golstein, P., Green, D. R., Hengartner, M., Knight, R. A., Kumar, S., Lipton, S. A., Malorni, W., Nunez, G., Peter, M. E., Tschopp, J., Yuan, J., Piacentini, M., Zhivotovsky, B. & Melino, G. (2009) Classification of cell death: recommendations of the Nomenclature Committee on Cell Death 2009, *Cell death and differentiation.* **16**, 3-11.

95. Klionsky, D. J.Abeliovich, H.Agostinis, P.Agrawal, D. K.Aliev, G.Askew, D. S.Baba, M.Baehrecke, E. H.Bahr, B. A.Ballabio, A.Bamber, B. A.Bassham, D. C.Bergamini, E.Bi, X.Biard-Piechaczyk, M.Blum, J. S.Bredesen, D. E.Brodsky, J. L.Brumell, J. H.Brunk, U. T.Bursch, W.Camougrand, N.Cebollero, E.Cecconi, F.Chen, Y.Chin, L. S.Choi, A.Chu, C. T.Chung, J.Clarke, P. G.Clark, R. S.Clarke, S. G.Clave, C.Cleveland, J. L.Codogno, P.Colombo, M. I.Coto-Montes, A.Cregg, J. M.Cuervo, A. M.Debnath, J.Demarchi, F.Dennis, P. B.Dennis, P. A.Deretic, V.Devenish, R. J.Di Sano, F.Dice, J. F.Difiglia, M.Dinesh-Kumar, S.Distelhorst, C. W.Djavaheri-Mergny, M.Dorsey, F. C.Droge, W.Dron, M.Dunn, W. A., Jr.Duszenko, M.Eissa, N. T.Elazar, Z.Esclatine, A.Eskelinen, E. L.Fesus, L.Finley, K. D.Fuentes, J. M.Fueyo, J.Fujisaki, K.Galliot, B.Gao, F. B.Gewirtz, D. A.Gibson, S. B.Gohla, A.Goldberg, A. L.Gonzalez, R.Gonzalez-Estevez, C.Gorski, S.Gottlieb, R. A.Haussinger, D.He, Y. W.Heidenreich, K.Hill, J. A.Hoyer-Hansen, M.Hu, X.Huang, W. P.Iwasaki, A.Jaattela, M.Jackson, W. T.Jiang, X.Jin, S.Johansen, T.Jung, J. U.Kadowaki, M.Kang, C.Kelekar, A.Kessel, D. H.Kiel, J. A.Kim, H. P.Kimchi, A.Kinsella, T. J.Kiselyov, K.Kitamoto, K.Knecht, E., et al. (2008) Guidelines for the use and interpretation of assays for monitoring autophagy in higher eukaryotes, *Autophagy.* **4**, 151-75.

96. North, B. J. & Verdin, E. (2007) Interphase nucleo-cytoplasmic shuttling and localization of SIRT2 during mitosis, *PLoS One.* **2**, e784.

97. Nie, H., Chen, H., Han, J., Hong, Y., Ma, Y., Xia, W. & Ying, W. (2011) Silencing of SIRT2 induces cell death and a decrease in the intracellular ATP level of PC12 cells, *International journal of physiology, pathophysiology and pharmacology.* **3**, 65-70.

98. Tang, X., Wang, Y., Zhou, S., Qian, T. & Gu, X. (2013) Signaling pathways regulating dose-dependent dual effects of TNF-alpha on primary cultured Schwann cells, *Molecular and cellular biochemistry.* **378**, 237-46.

99. Tao, T., Ji, Y., Cheng, C., Yang, H., Liu, H., Sun, L., Qin, Y., Yang, J., Wang, H. & Shen, A. (2009) Tumor necrosis factor-alpha inhibits Schwann cell proliferation by up-regulating Src-suppressed protein kinase C substrate expression, *Journal of neurochemistry.* **111**, 647-55.

100. Yuan, Q., Yang, H., Cheng, C., Li, C., Wu, X., Huan, W., Sun, H., Zhou, Z., Wang, Y., Zhao, Y., Lu, X. & Shen, A. (2012) beta-1,4-Galactosyltransferase I involved in Schwann cells proliferation and apoptosis induced by tumor necrosis factor-alpha via the activation of MAP kinases signal pathways, *Molecular and cellular biochemistry.* **365**, 149-58.

101. Dan, L., Klimenkova, O., Klimiankou, M., Klusman, J. H., van den Heuvel-Eibrink, M. M., Reinhardt, D., Welte, K. & Skokowa, J. (2012) The role of sirtuin 2 activation by nicotinamide phosphoribosyltransferase in the aberrant proliferation and survival of myeloid leukemia cells, *Haematologica.* **97**, 551-9.

102. Maxwell, M. M., Tomkinson, E. M., Nobles, J., Wizeman, J. W., Amore, A. M., Quinti, L., Chopra, V., Hersch, S. M. & Kazantsev, A. G. (2011) The Sirtuin 2 microtubule deacetylase is an abundant neuronal protein that accumulates in the aging CNS, *Human molecular genetics.* **20**, 3986-96.

103. Harting, K. & Knoll, B. (2010) SIRT2-mediated protein deacetylation: An emerging key regulator in brain physiology and pathology, *European journal of cell biology.* **89**, 262-9.

104. Zuo, Q., Wu, W., Li, X., Zhao, L. & Chen, W. (2012) HDAC6 and SIRT2 promote bladder cancer cell migration and invasion by targeting cortactin, *Oncology reports.* **27**, 819-24.

105. Burns, S. S., Akhmametyeva, E. M., Oblinger, J. L., Bush, M. L., Huang, J., Senner, V., Chen, C. S., Jacob, A., Welling, D. B. & Chang, L. S. (2013) Histone deacetylase inhibitor AR-42 differentially affects cell-cycle transit in meningeal and meningioma cells, potently inhibiting NF2-deficient meningioma growth, *Cancer research.* **73**, 792-803.

106. Bush, M. L., Oblinger, J., Brendel, V., Santarelli, G., Huang, J., Akhmametyeva, E. M., Burns, S. S., Wheeler, J., Davis, J., Yates, C. W., Chaudhury, A. R., Kulp, S., Chen, C. S., Chang, L. S., Welling, D. B. & Jacob, A. (2011) AR42, a novel histone deacetylase inhibitor, as a potential therapy for vestibular schwannomas and meningiomas, *Neuro-oncology.* **13**, 983-99.

107. Jacob, A., Oblinger, J., Bush, M. L., Brendel, V., Santarelli, G., Chaudhury, A. R., Kulp, S., La Perle, K. M., Chen, C. S., Chang, L. S. & Welling, D. B. (2012) Preclinical validation of AR42, a novel histone deacetylase inhibitor, as treatment for vestibular schwannomas, *The Laryngoscope.* **122**, 174-89.

108. Chen, C. S., Weng, S. C., Tseng, P. H., Lin, H. P. & Chen, C. S. (2005) Histone acetylation-independent effect of histone deacetylase inhibitors on Akt through the reshuffling of protein phosphatase 1 complexes, *The Journal of biological chemistry.* **280**, 38879-87.

109. Blakeley, J. O., Evans, D. G., Adler, J., Brackmann, D., Chen, R., Ferner, R. E., Hanemann, C. O., Harris, G., Huson, S. M., Jacob, A., Kalamarides, M., Karajannis, M. A., Korf, B. R., Mautner, V. F., McClatchey, A. I., Miao, H., Plotkin, S. R., Slattery, W., 3rd, Stemmer-Rachamimov, A. O., Welling, D. B., Wen, P. Y., Widemann, B., Hunter-Schaedle, K. & Giovannini, M. (2012) Consensus recommendations for current treatments and accelerating clinical trials for patients with neurofibromatosis type 2, *American journal of medical genetics Part A.* **158A**, 24-41.

110. Okada, T., Lopez-Lago, M. & Giancotti, F. G. (2005) Merlin/NF-2 mediates contact inhibition of growth by suppressing recruitment of Rac to the plasma membrane, *J Cell Biol.* **171**, 361-71.

111. Rodgers, G. M., 3rd, Becker, P. S., Bennett, C. L., Cella, D., Chanan-Khan, A., Chesney, C., Cleeland, C., Coccia, P. F., Djulbegovic, B., Garst, J. L., Gilreath, J. A., Kraut, E. H., Lin, W. C., Matulonis, U., Millenson, M., Reinke, D., Rosenthal, J., Sabbatini, P., Schwartz, R. N., Stein, R. S., Vij, R. & National Comprehensive Cancer, N. (2008) Cancer- and chemotherapy-induced anemia, *Journal of the National Comprehensive Cancer Network : JNCCN.* **6**, 536-64.

112. Pendergrass, K. B. (1998) Options in the treatment of chemotherapy-induced emesis, *Cancer practice.* **6**, 276-81.

113. Trueb, R. M. (2009) Chemotherapy-induced alopecia, *Seminars in cutaneous medicine and surgery.* **28**, 11-4.

114. Harrison, B. A., Whitlock, N. A., Voronkov, M. V., Almstead, Z. Y., Gu, K. J., Mabon, R., Gardyan, M., Hamman, B. D., Allen, J., Gopinathan, S., McKnight, B.,

Crist, M., Zhang, Y., Liu, Y., Courtney, L. F., Key, B., Zhou, J., Patel, N., Yates, P. W., Liu, Q., Wilson, A. G., Kimball, S. D., Crosson, C. E., Rice, D. S. & Rawlins, D. B. (2009) Novel class of LIM-kinase 2 inhibitors for the treatment of ocular hypertension and associated glaucoma, *Journal of medicinal chemistry.* **52**, 6515-8.

115. Hanahan, D. & Weinberg, R. A. (2011) Hallmarks of cancer: the next generation, *Cell.* **144**, 646-74.

116. Kaeberlein, M., McVey, M. & Guarente, L. (1999) The SIR2/3/4 complex and SIR2 alone promote longevity in Saccharomyces cerevisiae by two different mechanisms, *Genes & development.* **13**, 2570-80.

117. Kennedy, B. K., Austriaco, N. R., Jr., Zhang, J. & Guarente, L. (1995) Mutation in the silencing gene SIR4 can delay aging in S. cerevisiae, *Cell.* **80**, 485-96.

118. Haigis, M. C. & Sinclair, D. A. (2010) Mammalian sirtuins: biological insights and disease relevance, *Annual review of pathology.* **5**, 253-95.

119. Malhotra, V. & Perry, M. C. (2003) Classical chemotherapy: mechanisms, toxicities and the therapeutic window, *Cancer Biol Ther.* **2**, S2-4.